JOURNAL OF PETROLOGY

Journal of Petrology, 2018, Vol. 59, No. 11, 2043–2060
doi: 10.1093/petrology/egy089
Advance Access Publication Date: 20 September 2018
Original Article

OXFORD

HP–UHP Metamorphic Belt in the East Kunlun Orogen: Final Closure of the Proto-Tethys Ocean and Formation of the Pan-North-China Continent

Shuguang Song [1]*, Hengzhe Bi[1], Shengsheng Qi[2], Liming Yang[1], Mark B. Allen[3], Yaoling Niu[3], Li Su[4] and Wufu Li[2]

[1]MOE Key Laboratory of Orogenic Belt and Crustal Evolution School of Earth and Space Sciences, Peking University, Beijing 100871, China; [2]Qinghai Bureau of Geological Survey, Xining 810012, China; [3]Department of Earth Sciences, Durham University, Durham DH1 3LE, UK; [4]Institute of Earth Science and State Key Laboratory of Geological Processes and Mineral Resources, Chinese University of Geosciences, Beijing 100083, China

*Corresponding author. E-mail: sgsong@pku.edu.cn

Received April 8, 2018; Accepted September 12, 2018

ABSTRACT

The East Kunlun Orogen, the northwestern part of the Central China Orogenic Belt, is a long-lived accretionary orogenic belt that records the evolution and eventual destruction of branches of the Tethys Ocean, from the Cambrian to the Triassic. Here we report an Early Paleozoic eclogite belt that extends for ~500 km within the East Kunlun Orogen. This belt consists of eclogite blocks, metasedimentary rocks and minor serpentinite blocks, accompanied by ophiolites (530–460 Ma) and concurrent arc volcanic sequences and granitic plutons. Geochemical data show that the eclogites have normal mid-ocean ridge basalt- to ocean island basalt-like compositions. U–Pb dating of metamorphic zircons from eclogites and their surrounding rocks gave peak and retrograde metamorphic ages of 430–410 Ma. Coesite pseudomorphs in garnet, quartz exsolution rods in omphacite and *P–T* calculations suggest that some eclogites experienced ultrahigh-pressure (UHP) metamorphic conditions at 29–30 kbar and 610–675°C; these could represent oceanic crust subducted to and exhumed from coesite-forming depths (100–120 km). The UHP metamorphic eclogite belt in the East Kunlun Orogen may represent the final closure of the Proto-Tethys Ocean (opening at ~580 Ma, subduction initiating at ~520 Ma) at ~430–410 Ma in the East Kunlun, with the formation of the Pan-North-China Continent in the Early Paleozoic and expansion of the Paleo-Tethys Ocean in the south.

Key words: eclogite belt; ultrahigh-pressure metamorphism; Proto-Tethys Ocean; East Kunlun Orogen

INTRODUCTION

Eclogites carry information that is critical in understanding orogenic processes (e.g. Ernst, 1988; Carswell, 1990; Ernst & Liou, 1995). Together with ophiolites, arc magmatism and the sedimentary fill of accretionary prisms, eclogites characterize orogenic belts associated with paleo-ocean subduction (e.g. Agard *et al.*, 2009; Song *et al.*, 2013) and provide valuable information on the processes and conditions of subduction and exhumation.

The Proto-Tethys Ocean is an inconsistently used concept for a supposed predecessor of the Paleo-Tethys Ocean, which separated some blocks (e.g. the Qaidam–Qilian, South China) from the northern margins of Gondwana in the Neoproterozoic (e.g. Li *et al.*, 2008; von Raumer & Stampfli, 2008; Xu *et al.*, 2015). The evolution of Proto-Tethys is, however, ambiguous concerning the timing of its opening and closing, as well as geological processes in the course of its shrinking and transition to the Paleo-Tethys Ocean.

The Qinling–Qilian–Kunlun orogenic belt (or the Central China Orogenic Belt) lies in the central part of China and is considered to have resulted from the consumption of the Proto-Tethys (e.g. Yin & Harrison, 2000; Dong & Santosh, 2016; Song *et al.*, 2017). The East Kunlun, the west part of the Qinling–Qilian–Kunlun Mountains (Fig. 1), is a long-lived orogenic belt with a history from Cambrian to Triassic times, which records the orogenic evolution of the Proto- and Paleo-Tethys oceans, and holds the key to understanding the evolution of the ancient Tethys Ocean and formation of the Chinese continent. Eclogite blocks were reported by Meng *et al.* (2013) and subsequently by Qi *et al.* (2016) at Wenquan in the east, and by Qi *et al.* (2014) at Xiarihamu in the west of the East Kunlun Orogen (EKO) (Fig. 1). With the addition of a newly discovered eclogite-bearing locality at Kehete in the mid-east, a 500 km long, eclogite-bearing high-pressure metamorphic belt can be recognized within the EKO. In this study, we present petrological, geochemical and geochronological studies of this eclogite belt. We have determined for the first time that some of the EKO eclogites have experienced UHP metamorphism in Silurian–Devonian times. This eclogite belt, together with accompanying ophiolites and arc volcanic rocks, represents the final closure of the Proto-Tethys Ocean, and continued convergence between fragments of Eastern Gondwanaland and the North China–Tarim continent.

Mineral abbreviations are after Whitney & Evans (2010).

GEOLOGICAL SETTING AND PETROGRAPHY

The East Kunlun Orogen lies south of the Qaidam Block (Fig. 1). The basement of the Qaidam Block is largely covered by thick sedimentary successions of a Mesozoic to Cenozoic intracontinental basin. The Precambrian crystalline basement is mainly exposed at the north and south margins of the block. To the north of the Qaidam Block is the North Qaidam ultrahigh-pressure metamorphic (UHPM) belt, which consists of various types of eclogite, garnet peridotite, coesite-bearing metapelite and granitic gneiss. The North Qaidam UHPM belt is a continental collision zone recording that the Qaidam Block had subducted northwards to depths of ~200 km at ~440–425 Ma (e.g. Song *et al.*, 2014, and references therein). Further north, the Qilian Orogen consists of the South Qilian oceanic accretionary belt, the Central Qilian Block and the North Qilian oceanic accretionary belt. The South Qilian oceanic accretionary belt (SQAB) is composed of Cambrian ophiolites (535–500 Ma) and an Ordovician intra-oceanic arc complex (470–440 Ma) (e.g. Song *et al.*, 2017; Zhang *et al.*, 2017), without high-pressure rocks. The North Qilian oceanic accretionary belt (NQAB) consists of 550–450 Ma ophiolites, 520–440 Ma continental arc volcanic and plutonic rocks and 500–440 Ma high-pressure metamorphic rocks. Carpholite in metapelites and lawsonite in eclogites and blueschists suggest relatively cold oceanic subduction and high-pressure/low-temperature (HP/LT) metamorphism (Song *et al.*, 2007; Zhang *et al.*, 2007). Therefore, three subparallel HP–UHP belts are exposed in a 400 km wide region in the northern Tibetan Plateau (Fig. 1). These HP–UHP belts, together with associated ophiolites and arc rocks, record the evolution of the northern Proto-Tethys Ocean from ocean-floor subduction and consumption to subsequent continental collision (Song *et al.*, 2006, 2014).

The East Kunlun Orogen records a long and complex history from Cambrian to Triassic times (Dong *et al.*,

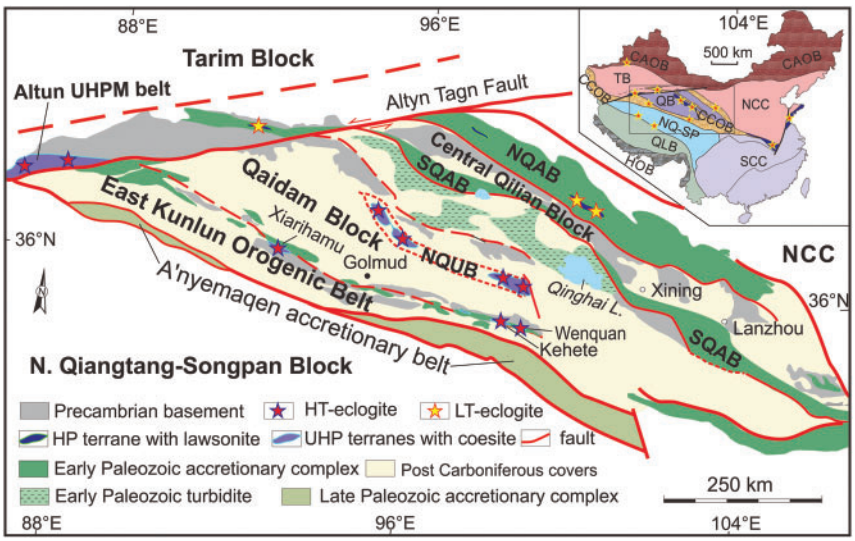

Fig. 1. Simplified geological map of the northern Tibetan Plateau showing HP–UHP metamorphic terranes in three orogenic belts. CAOB, Central Asian Orogenic Belt; CCOB, Central China Orogenic Belt; HOB, Himalayan Orogenic Belt; NCC, North China Craton; NQ-SP, North Qiangtang–Songpan Block; SCC, South China Craton; QLB, Qiangtang–Lhasa Block; TB, Tarim Block; NQAB, North Qilian Accretionary Belt; SQAB, South Qilian Accretionary Belt; NQUB, North Qaidam UHPM Belt; EKO, East Kunlun Orogen; CQB, Central Qilian Block.

2018; Li *et al.*, 2018). It mainly consists of (1) an Early Paleozoic accretionary complex at the southwestern margin of the Qaidam Block, (2) the A'nyemaqen accretionary complex in the south, (3) Precambrian basement (the South Kunlun Block), and (4) Triassic volcanic and plutonic rocks distributed throughout the East Kunlun Orogen. Ophiolites in the Early Paleozoic accretionary complex formed over a long period from 537 to 460 Ma (Yang *et al.*, 1996; Bian *et al.*, 2004; Meng *et al.*, 2015; Qi *et al.*, 2016; Li *et al.*, 2018), the same as ophiolites in the Qilian–Qaidam region to the north (Song *et al.*, 2013). The types of ophiolite are not well documented, partly because most ophiolites are strongly deformed and fragmented. Basalts with pillow structure show characteristics of normal- to enriched-mid-ocean ridge basalt (N- to E-MORB) affinity (Yang *et al.*, 1996; Qi *et al.*, 2016), most probably representative of MORB-type ophiolites (e.g. Topuz *et al.*, 2018). Arc volcanic rocks include Alaskan-type ultramafic–mafic intrusions with Cu–Ni ore-deposits, andesites–rhyolites and granites with Silurian–Devonian ages (450–400 Ma) (e.g. Zhu *et al.*, 2006; Wang *et al.*, 2014). Three eclogite-bearing regions, from east to west Wenquan, Kehete and Xiarihamu, are distributed discontinuously along the Early Paleozoic accretionary belt (Fig. 1). The A'nyemaqen accretionary complex in the south is mainly a mélange belt with 460–308 Ma ophiolitic fragments (Bian *et al.*, 2004; Yang *et al.*, 2004). The Precambrian basement in the EKO mainly consists of 1200–950 Ma Mesoproterozoic granitic gneisses. Detrital zircons from metapelite (KL33) yielded an age peak at 2482 Ma, with secondary age groups of 2686–2505 and 2180–1054 Ma; detrital zircons from late Neoproterozoic sedimentary rocks (Golmud region) yield a major age group of 1465–802 Ma and three minor age groups of 1892–1758, 2502–2431 and 3308 Ma (author's unpublished data).

All eclogites in the three terranes occur as lens-shaped blocks of varying size (5–100 m in length) within metasedimentary hosts, including metapelite and marble (Fig. 2a–d). A serpentinite block has also been

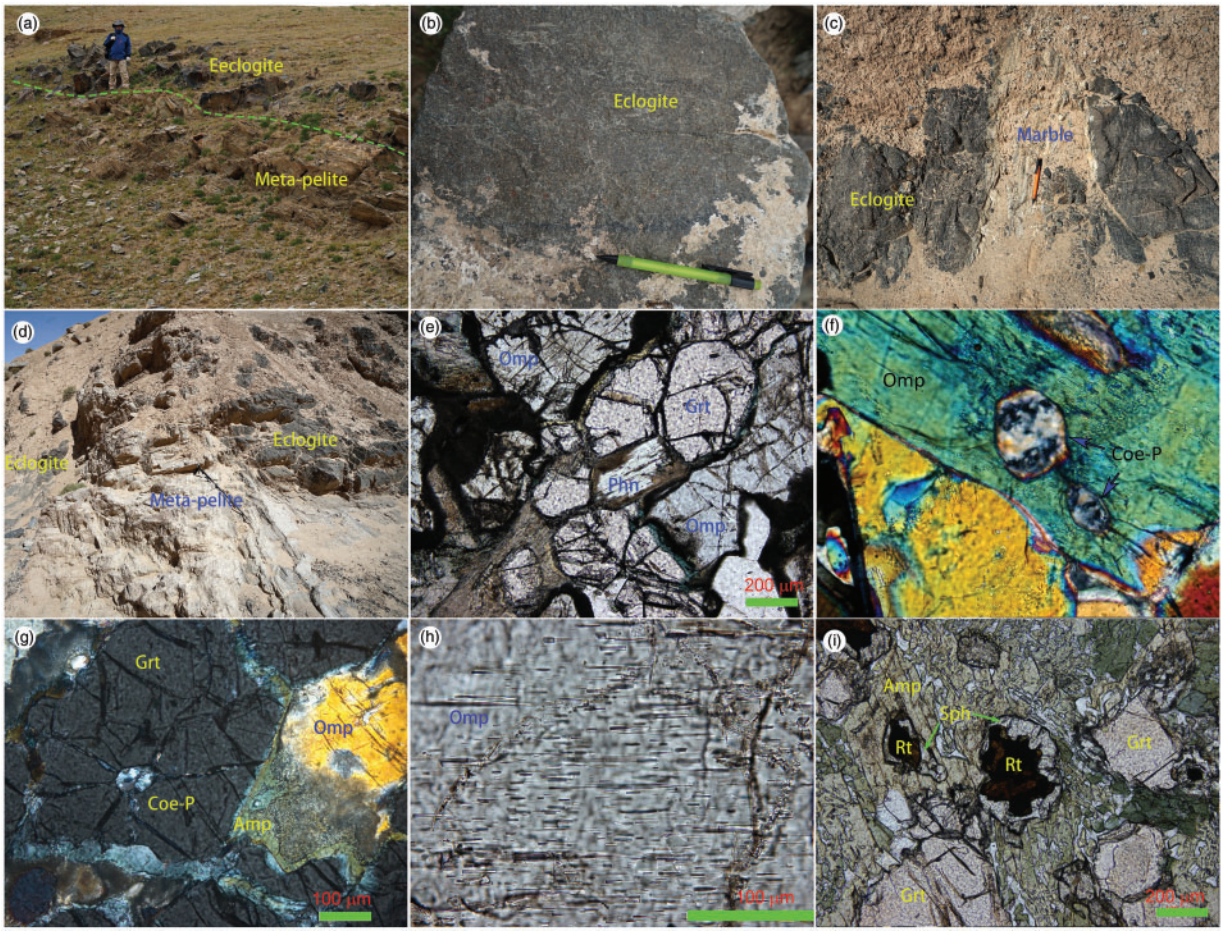

Fig. 2. Field photographs and photomicrographs of the eclogite belt in the EKO. (a) Eclogite block within garnet–mica schist (metapelite) from Kehete terrane. (b) Eclogite block with weak alteration (Kehete terrane). (c) Eclogite blocks with marble (Xiarihamu terrane). (d) Eclogite blocks within metapelite (Xiarihamu terrane). (e) Photomicrograph of eclogite with the mineral assemblage garnet (Grt), omphacite (Omp), phengite (Phn), rutile (Rt) and quartz (16KL13). (f) Coesite-pseudomorphs (Coe-P) in omphacite. (g) Coesite-pseudomorph (Coe-P) in garnet. [Note Omp rims decompressed into symplectitic low-Na clinopyroxene (Cpx) and oligoclase (Oli) and further replaced by amphibole (Amp).] (h) Densely packed quartz exsolution rods in Omp. (i) Amphibolite-facies retrogression of eclogite in the Xiarihamu terrane, with omphacite replaced by amphibole and rutile (Rt) by titanite (Ttn).

discovered in the Kehete terrane. The metapelite samples have a schistose structure, with red grains of garnet and foliated mica in outcrop. The rocks are composed of garnet (5–15%), muscovite (20–30%), biotite (5–10%), quartz (35–45%), plagioclase (~10%) and minor tourmaline, zircon, and rutile. Most rutile grains in the matrix are replaced by titanite and/or ilmenite. No granitic gneiss has been found in the eclogite-bearing high-pressure terranes. The rock assemblage, plus some serpentinite massifs, suggests an oceanic-type subduction mélange.

Most eclogite samples in the east section of the HP–UHP belt are fresh. They show granoblastic textures with a mineral assemblage of garnet, omphacite, rutile, quartz and minor phengite, without obvious foliation. Garnet occurs as euhedral crystals with rare zircon and rutile inclusions (Fig. 2e and f). Coesite pseudomorphs are observed as inclusions in garnet (Fig. 2g). Most omphacite crystals contain densely packed oriented quartz rods (Fig. 2h). Omphacite crystals are commonly replaced by Cpx + Oli symplectites and further by amphibole, and rutile is replaced by titanite, suggesting that these eclogite samples are overprinted by later decompression and amphibolite-facies retrogression (Fig. 2i).

ANALYTICAL METHODS

Mineral compositions

Polished thin sections were produced from representative pieces of the studied samples, and were examined in detail using a petrographic microscope. Mineral compositions were analysed using an electron probe microanalyzer (EPMA) (JEOL JXA-8100) at Peking University, operated at 15 kV acceleration voltage, with 20 nA beam current and 1–5 μm beam spot. Routine analyses were obtained by counting for 20 s at peak and 5 s on background. Synthetic silica (Si) and spessartine (Mn), natural sanidine (K), pyrope (Mg), andradite (Fe and Ca), albite (Na and Al) and rutile (Ti) were used as standards. Ferric iron in minerals was determined based on the scheme of Droop (1987).

Whole-rock major and trace elements

On the basis of careful petrographic observations, we selected 18 samples for whole-rock major and trace element analyses. The whole-rock major element oxides were analyzed using a Leeman Prodigy inductively coupled plasma optical emission spectroscopy system (ICP-OES) at the China University of Geosciences, Beijing (CUGB). The analytical precisions (1σ) for most major elements based on master standards GSR-1, GSR-3, GSR-5 (national geological standard reference materials of China) and USGS AGV-2 are better than 1%, except for TiO_2 (~1·5%) and P_2O_5 (~2·0%). Loss on ignition (LOI) was determined by placing 1 g of sample powder in a furnace at 1000°C for several hours before being cooled in a desiccator and reweighed (Song *et al.*, 2010).

The trace element compositions of Haolaoluchang volcanic samples were determined by inductively coupled plasma mass spectrometry (ICP-MS) using an Agilent-7500a quadrupole system in the Institute of Earth Science, CUGB. About 40 mg power for each sample was dissolved in a distilled acid mixture (1:1 HNO_3–HF) in a Teflon digesting vessel and heated on a hotplate at 185°C for 48 h, using high-pressure bombs for digestion–dissolution. The sample was then evaporated to incipient dryness, refluxed with 1 ml 6N HNO_3, and heated again to incipient dryness. The sample was again dissolved in 2 ml of 3N HNO_3 in a high-pressure bomb at 165°C for a further 24 h to ensure complete dissolution. Such digested samples were finally diluted with Milli-Q water to a dilution factor of 2000 in 2% HNO_3 solution for analysis. Master standards (GSR-1, GSR-3, GSR-5 and USGS AGV-2) were used to monitor the analytical accuracy and precision. Analytical accuracy, as indicated by a relative difference between measured and recommended values, is better than 5% for most elements, and 10–15% for Cu, Zn, Gd, and Ta.

Zircon preparation and U–Th–Pb analysis

The samples were crushed and sieved to ~300 μm for the first separation and then to ~100 μm for the second separation. Zircons were separated by combining magnetic and heavy liquid methods before finally hand-picking under a binocular microscope. Zircon grains, together with zircon standard 91500, were mounted in epoxy mounts, which were then polished to section the crystals in half for analysis. All zircons were documented with transmitted and reflected light micrographs as well as cathodoluminescence (CL) images to reveal their internal structures, and the mount was vacuum-coated with high-purity gold prior to secondary ion mass spectrometry (SIMS) analysis. The CL images were obtained on an FEI Philips XL30 SFEG SEM with 2 min scanning time at conditions of 15 kV and 20 nA at Peking University.

Measurements of U, Th and Pb were conducted using the Cameca IMS-1280 SIMS system at the Institute of Geology and Geophysics, Chinese Academy of Sciences in Beijing. U–Th–Pb ratios and absolute abundances were determined relative to the standard zircon 91500 (Wiedenbeck *et al.*, 1995), analyses of which were interspersed with those of unknown grains, using operating and data processing procedures similar to those described by Li *et al.* (2009). A long-term uncertainty of 1·5% (1RSD) for $^{206}Pb/^{238}U$ measurements of the standard zircons was propagated to the unknowns (Li *et al.*, 2010), despite the fact that the measured $^{206}Pb/^{238}U$ error in a specific session is generally around 1% (1RSD) or less. Measured compositions were corrected for common Pb using non-radiogenic ^{204}Pb. Corrections are sufficiently small to be insensitive to the choice of common Pb composition, and an average of the present-day crustal composition (Stacey & Kramers, 1975) was used for the common Pb, assuming that the

Table 1: Representative analyses of garnet in eclogites from Kehete Terane (HKT) and Xiarihamu Terrane, East Kunlun Orogen

Sample:	16KL13-1	16KL13-2	16KL26-1	16KL26-2	16KL27-1	16KL27-2	16KL27-3	16KL27A-1	16KL27A-2	16KL27A-3	14k2-1	14k2-2	14k2-3	14k4-1	14k4-2	14k4-3	14k5-1	14k5-2	14k5-3
Location:	HKT	HKT	HKT	HKT	HKT	HKT	HKT	HKT	HKT	HKT	XRHM	XRHM	XRHM	XRHM	XRHM	XRHM	XRHM	XRHM	XRHM
SiO_2	37·66	38·73	37·93	38·32	38·63	38·81	38·45	38·18	38·39	38·45	38·94	36·77	37·93	38·93	38·48	38·42	39·16	38·82	39·29
TiO_2	0·12	0·11	0·07	0·10	0·11	0·01	0·08	0·03	0·07	0·05	0·05	0·14	0·10	0·13	0·07	0·16	0·00	0·11	0·07
Al_2O_3	21·06	21·28	20·87	21·71	21·71	21·36	21·47	21·50	21·31	21·42	22·20	21·19	22·23	21·83	21·51	21·73	22·23	22·31	22·46
Cr_2O_3	0·01	0·07	0·00	0·01	0·00	0·03	0·04	0·01	0·00	0·04	0·02	0·00	0·06	0·00	0·00	0·02	0·04	0·01	0·01
FeO	26·55	22·24	25·89	26·21	21·89	22·09	22·28	23·17	23·14	22·88	25·48	25·86	25·96	25·96	28·70	28·06	25·71	23·69	24·63
MnO	0·53	0·40	0·50	0·36	0·48	0·40	0·50	0·51	0·47	0·42	0·27	0·54	0·76	0·45	0·56	0·35	0·09	0·85	0·05
NiO	0·05	0·00	0·00	0·10	0·00	0·03	0·00	0·05	0·00	0·00	0·00	0·04	0·00	0·04	0·02	0·04	0·03	0·00	0·00
MgO	5·00	7·02	7·14	7·19	7·06	6·95	6·83	6·73	6·80	6·70	3·34	2·04	2·08	4·33	2·34	3·13	3·72	3·53	3·80
CaO	8·28	9·57	6·55	6·27	9·87	9·99	9·12	8·91	9·38	9·65	11·09	12·05	12·19	9·56	10·06	9·91	10·04	12·09	11·33
Na_2O	0·06	0·06	0·04	0·05	0·05	0·05	0·00	0·08	0·03	0·01	0·00	0·01	0·00	0·06	0·00	0·00	0·05	0·00	0·00
K_2O	0·01	0·00	0·00	0·01	0·00	0·00	0·00	0·03	0·00	0·01	0·00	0·00	0·00	0·01	0·00	0·03	0·00	0·00	0·00
Total	99·33	99·48	99	100·32	99·8	99·73	98·77	99·2	99·59	99·62	101·4	98·62	101·31	101·29	101·74	101·85	101·06	101·41	101·64
Calculation using 12 oxygen																			
Si	2·962	2·987	2·964	2·952	2·966	2·985	2·991	2·961	2·966	2·969	3·008	2·944	2·953	3·003	2·999	2·976	3·030	2·988	3·015
Ti	0·007	0·006	0·004	0·006	0·006	0·001	0·005	0·002	0·004	0·003	0·003	0·008	0·006	0·008	0·004	0·009	0·000	0·006	0·004
Al	1·952	1·934	1·922	1·971	1·964	1·936	1·968	1·965	1·940	1·949	2·021	1·999	2·039	1·985	1·976	1·984	2·027	2·023	2·031
Cr	0·001	0·004	0·000	0·001	0·000	0·002	0·002	0·001	0·000	0·002	0·001	0·000	0·004	0·000	0·000	0·001	0·002	0·001	0·001
Fe^{3+}	0·120	0·083	0·149	0·120	0·099	0·098	0·039	0·125	0·124	0·107	0·000	0·098	0·039	0·004	0·017	0·047	0·000	0·000	0·000
Fe^{2+}	1·626	1·352	1·542	1·568	1·306	1·323	1·410	1·378	1·371	1·370	1·646	1·633	1·650	1·671	1·853	1·770	1·664	1·525	1·580
Mn	0·035	0·026	0·033	0·024	0·031	0·026	0·033	0·034	0·031	0·028	0·018	0·037	0·050	0·029	0·037	0·023	0·006	0·055	0·003
Ni	0·003	0·000	0·000	0·006	0·000	0·002	0·000	0·003	0·000	0·000	0·000	0·003	0·000	0·002	0·001	0·002	0·002	0·000	0·000
Mg	0·586	0·807	0·832	0·826	0·808	0·797	0·792	0·778	0·783	0·771	0·385	0·243	0·241	0·498	0·272	0·361	0·429	0·405	0·435
Ca	0·698	0·791	0·548	0·518	0·812	0·823	0·760	0·740	0·776	0·798	0·918	1·033	1·017	0·790	0·840	0·822	0·832	0·997	0·931
Na	0·009	0·009	0·006	0·007	0·007	0·007	0·000	0·012	0·004	0·001	0·000	0·002	0·000	0·009	0·000	0·000	0·008	0·000	0·000
K	0·001	0·000	0·000	0·001	0·000	0·000	0·000	0·003	0·000	0·001	0·000	0·000	0·000	0·001	0·000	0·003	0·000	0·000	0·000
Sum	8	8	8	8	8	8	8	8	8	8	8	8	8	8	8	8	8	8	8
Pyrope	19·13	26·39	26·79	27·03	26·44	25·98	26·10	25·47	25·39	25·09	12·97	8·00	8·05	16·64	9·01	11·95	14·64	13·58	14·74
Alm	56·96	46·90	54·48	55·26	45·98	46·32	47·76	49·19	48·45	48·05	55·49	56·86	56·36	55·97	61·95	60·10	56·76	51·13	53·58
Spess	1·15	0·86	1·07	0·77	1·02	0·85	1·09	1·10	1·00	0·89	0·60	1·20	1·67	0·98	1·23	0·76	0·20	1·86	0·11
Uvaro	0·03	0·22	0·00	0·03	0·00	0·09	0·12	0·03	0·00	0·13	0·06	0·00	0·18	0·00	0·00	0·06	0·12	0·03	0·03
Grossular	22·73	25·63	17·66	16·91	26·56	26·75	24·92	24·20	25·16	25·84	30·88	33·94	33·73	26·41	27·82	27·13	28·28	33·40	31·55

Fe^{3+} in garnet and clinopyroxene was calculated by charge balance after Droop (1987).

Table 2: Representative analyses of omphacite in eclogites from Kehete Terane (KHT) and Xiarihamu Terrane, East Kunlun Orogen

Sample:	16KL13-1	16KL13-2	16KL13-3	16KL27-1	16KL27-2	16KL27A-1	16KL27A-2	16KL26-1	16KL26-2	14k2-1	14k4-1	14k4-2	14k4-3	14k4-5	k4-5·1	k4-6·1	k4-7·5	XR1-1	XR2-1
Location:	HKT	HKT	HKT	HKT	HKT	HKT	HKT	HKT	HKT	XRHM	XRHM	XRHM	XRHM	XRHM	XRHM	XRHM	XRHM	XRHM	XRHM
SiO_2	56·05	55·40	55·33	55·31	55·37	55·31	55·39	55·44	55·24	54·85	51·73	52·42	54·88	55·31	54·56	52·62	52·79	54·69	53·99
TiO_2	0·09	0·17	0·10	0·10	0·05	0·14	0·21	0·11	0·16	0·13	0·06	0·07	0·07	0·09	0·12	0·06	0·10	0·14	0·16
Al_2O_3	9·32	9·89	9·69	10·01	9·49	9·83	9·08	9·11	9·05	5·71	4·72	4·56	5·49	5·21	5·37	3·13	4·72	7·80	8·10
Cr_2O_3	0·04	0·00	0·00	0·00	0·03	0·00	0·00	0·00	0·06	0·07	0·01	0·04	0·00	0·00	0·05	0·00	0·07	0·03	0·06
FeO	6·47	6·53	6·30	6·88	4·57	4·42	6·21	6·02	6·04	6·99	14·11	10·30	8·23	7·60	8·54	10·43	9·41	5·33	5·09
MnO	0·03	0·09	0·02	0·06	0·00	0·03	0·03	0·02	0·02	0·10	0·10	0·02	0·08	0·00	0·01	0·09	0·01	0·06	0·02
NiO	0·00	0·05	0·00	0·06	0·05	0·00	0·00	0·00	0·00	0·00	0·07	0·00	0·06	0·06	0·00	0·00	0·00	0·06	0·00
MgO	7·33	7·35	7·16	7·52	9·22	9·20	9·11	8·83	8·85	11·56	10·58	10·32	10·36	10·67	10·66	11·47	10·72	9·98	10·10
CaO	13·60	13·69	13·67	12·50	14·85	14·51	13·66	13·75	13·78	18·73	17·51	19·30	17·51	17·90	17·29	21·33	18·28	15·80	15·94
Na_2O	6·74	6·58	6·96	6·83	5·99	6·29	6·36	6·20	6·42	2·17	1·54	2·58	3·64	3·67	3·82	1·37	3·37	5·30	5·69
K_2O	0·04	0·02	0·01	0·01	0·00	0·01	0·00	0·02	0·00	0·03	0·01	0·00	0·00	0·03	0·00	0·01	0·00	0·00	0·01
Total	99·72	99·76	99·24	99·28	99·61	99·74	100·05	99·49	99·62	100·35	100·45	99·6	100·22	100·53	100·42	100·5	99·47	99·19	99·17
Calculation using 6 oxygen																			
Si	2·016	1·993	1·995	1·995	1·982	1·972	1·978	1·993	1·981	2·009	1·937	1·949	2·002	2·008	1·984	1·953	1·947	1·977	1·943
Ti	0·002	0·005	0·003	0·003	0·001	0·004	0·006	0·003	0·004	0·004	0·002	0·002	0·002	0·002	0·003	0·002	0·003	0·004	0·004
Al	0·395	0·419	0·412	0·426	0·400	0·413	0·382	0·386	0·382	0·246	0·208	0·200	0·236	0·223	0·230	0·137	0·205	0·332	0·344
Cr	0·001	0·000	0·000	0·000	0·001	0·000	0·000	0·000	0·002	0·002	0·000	0·001	0·000	0·000	0·001	0·000	0·002	0·001	0·002
Fe^{3+}	0·0378	0·0445	0·0797	0·0569	0·0478	0·0706	0·0909	0·0544	0·0917	0·0000	0·0260	0·0826	0·0140	0·0151	0·0628	0·0528	0·1344	0·077	0·153
Fe^{2+}	0·157	0·152	0·110	0·151	0·089	0·061	0·095	0·127	0·089	0·214	0·416	0·238	0·237	0·216	0·197	0·271	0·156	0·085	0·000
Mn	0·001	0·003	0·001	0·002	0·000	0·001	0·001	0·001	0·001	0·003	0·003	0·001	0·002	0·000	0·000	0·003	0·000	0·002	0·001
Ni	0·000	0·001	0·000	0·002	0·001	0·000	0·000	0·000	0·000	0·000	0·002	0·000	0·002	0·002	0·000	0·000	0·000	0·002	0·000
Mg	0·393	0·394	0·385	0·404	0·492	0·489	0·485	0·473	0·473	0·631	0·591	0·572	0·563	0·578	0·578	0·635	0·589	0·538	0·542
Ca	0·524	0·528	0·528	0·483	0·569	0·554	0·523	0·530	0·529	0·735	0·702	0·769	0·684	0·696	0·674	0·848	0·722	0·612	0·615
Na	0·470	0·459	0·487	0·478	0·416	0·435	0·440	0·432	0·446	0·154	0·112	0·186	0·257	0·258	0·269	0·099	0·241	0·371	0·397
K	0·002	0·001	0·000	0·000	0·000	0·000	0·000	0·001	0·000	0·001	0·000	0·000	0·000	0·001	0·000	0·000	0·000	0·000	0·000
Sum	4	4	4	4	4	4	4	4	4	4	4	4	4	4	4	4	4	4	4
Jd	41·41	41·74	40·95	42·34	38·37	38·88	36·58	38·24	36·77	25·91	14·72	15·10	23·97	23·38	21·76	9·16	15·48	31·32	29·07
Ae	3·78	4·45	7·97	5·69	4·78	7·06	9·09	5·44	9·17	0·00	2·60	8·26	1·40	1·51	6·28	5·28	13·44	7·65	15·32
WEF	54·81	53·81	51·08	51·97	56·85	54·06	54·33	56·32	54·06	74·09	82·69	76·64	74·63	75·11	71·96	85·56	71·08	61·03	55·61

Fe^{3+} in garnet and clinopyroxene was calculated by charge balance (Droop, 1987).

common Pb is largely surface contamination introduced during sample preparation. Uncertainties on individual analyses in data tables are reported at a 1σ level; mean ages for pooled U/Pb (and Pb/Pb) analyses are quoted with a 95% confidence interval. Data reduction was carried out using the Isoplot/Ex v. 2.49 program (Ludwig, 2003).

Measurements of U–Pb in zircons by laser ablation (LA)-ICP-MS were carried out on an Agilent-7500a quadrupole ICP-MS system coupled with a New Wave SS UP193 laser sampler at the China University of Geosciences, Beijing. Laser spot size of 36 μm, laser energy density of 8·5 J cm^{-2} and a repetition rate of 10 Hz were applied for analysis. National Institute of Standards and Technology 610 glass and zircon standard 91500 (Wiedenbeck *et al.*, 1995) were used as external standards, Si as an internal standard, and zircon standard Qinghu zircon as the secondary standard. The software GLITTER (ver. 4.4, Macquarie University) was used to process the isotopic ratios and element concentrations of zircons. The common lead correction was made following Andersen (2002). Age calculations and plots of concordia diagrams were made using Isoplot/Ex v. 3.0 program (Ludwig, 2003). Analytical details have been described by Song *et al.*, (2010).

Table 3: Representative analyses of phengite in eclogites from Kehete Terane, East Kunlun Orogen

Sample:	16KL13-1	16KL27-1	16KL27-1	16KL27-1	16KL27A-1
SiO_2	55·96	53·42	52·48	53·24	54·65
TiO_2	0·94	0·69	0·67	0·73	0·68
Al_2O_3	24·88	26·99	27·78	28·04	26·11
Cr_2O_3	0·00	0·07	0·02	0·06	0·00
FeO	1·63	2·00	1·97	1·74	1·78
MnO	0·02	0·03	0·01	0·00	0·01
NiO	0·02	0·00	0·01	0·02	0·02
MgO	4·76	3·95	3·14	3·52	4·16
CaO	0·00	0·02	0·02	0·03	0·01
Na_2O	0·12	0·36	0·31	0·61	0·38
K_2O	8·60	9·24	8·95	8·02	8·72
Total	96·93	96·76	96·37	96·01	96·52
Calculation using 12 oxygen					
Si	3·591	3·466	3·447	3·452	3·533
Ti	0·045	0·034	0·033	0·036	0·033
Al	1·882	2·064	2·150	2·142	1·989
Cr	0·000	0·004	0·001	0·003	0·000
Fe	0·087	0·109	0·108	0·094	0·096
Mn	0·001	0·002	0·001	0·000	0·001
Ni	0·001	0·000	0·001	0·001	0·001
Mg	0·455	0·382	0·307	0·340	0·401
Ca	0·000	0·001	0·001	0·002	0·001
Na	0·015	0·045	0·039	0·077	0·048
K	0·704	0·765	0·750	0·663	0·719
Sum	6·782	6·871	6·839	6·810	6·822

MINERAL AND WHOLE-ROCK CHEMISTRY

Chemical compositions of representative metamorphic minerals are listed in Tables 1–3. Garnets in eclogites from the three eclogite terranes show varying compositions (Fig. 3a). Eclogitic garnets in the Kehete terrrane are homogeneous in composition, whereas garnets in eclogites from the Xiarihamu terrane display weak

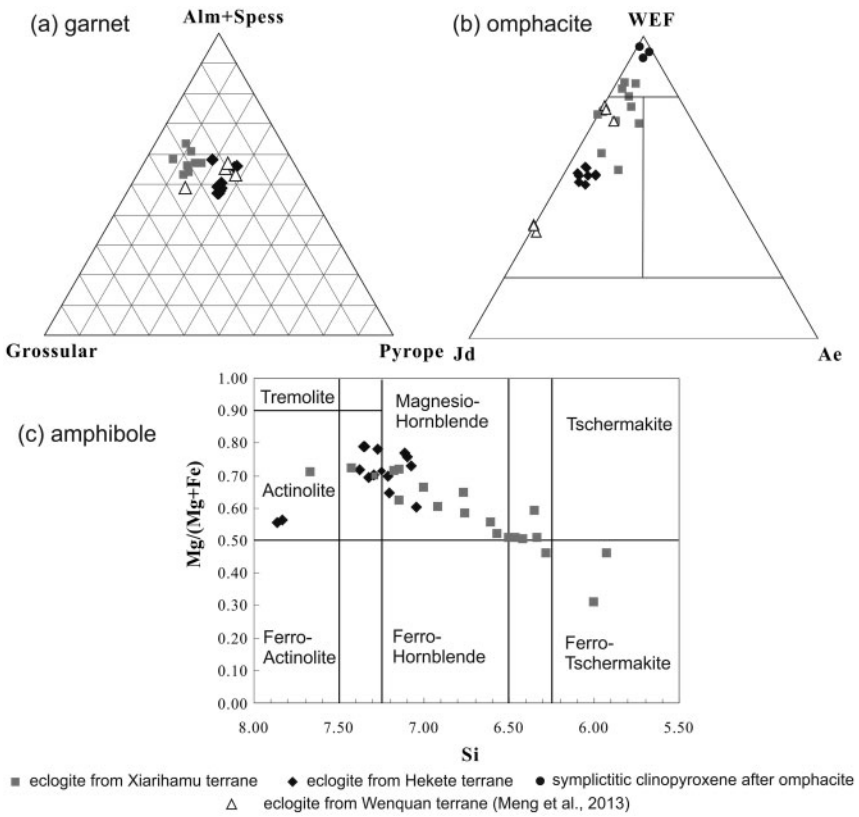

Fig. 3. Diagrams showing compositional variation of garnet (a), clinopyroxene (b) and amphibole (c) from the East Kunlun eclogite belt.

Table 4: Representative analyses of amphibole in eclogites from Kehete (KHT) and Xiarihamu (XRHM) terranes, East Kunlun Orogen

Sample:	16KL02	16KL09	16KL10-1	16KL10-2	16KL-8-1	16KL04-1	16KL04-2	16KL05-1	16KL05-2	16KL11-1	16KL11-2	14k2-1	14k2-2	14k2-3	14k2-4	14k5-1	14k5-2	k5-2.4
Location:	KHT	KHT	KHT	KHT	KHT	KHT	KHT	KHT	KHT	KHT	KHT	XRHM	XRHM	XRHM	XRHM	XRHM	XRHM	XRHM
SiO_2	49·81	50·89	52·60	53·06	49·52	50·13	48·97	51·65	51·72	50·19	47·36	50·75	52·14	42·97	48·19	49·86	53·45	42·79
TiO_2	0·13	0·13	0·14	0·02	0·14	0·16	0·28	0·14	0·26	0·14	0·15	0·25	0·44	0·16	0·28	0·24	0·06	0·29
Al_2O_3	7·31	6·18	1·48	1·47	7·33	6·55	7·89	6·21	6·23	6·48	8·33	6·78	5·59	12·75	8·90	8·12	3·50	15·02
Cr_2O_3	0·15	0·05	0·00	0·00	0·00	0·01	0·06	0·03	0·08	0·04	0·02	0·00	0·05	0·02	0·02	0·01	0·00	0·08
FeO	10·82	10·70	16·95	17·53	11·66	11·42	12·72	8·29	8·18	12·30	14·85	11·49	10·66	17·57	13·32	10·68	11·85	13·39
MnO	0·05	0·00	0·45	0·33	0·14	0·10	0·07	0·04	0·09	0·09	0·06	0·07	0·09	0·00	0·06	0·10	0·05	0·07
NiO	0·00	0·00	0·03	0·00	0·00	0·03	0·09	0·08	0·00	0·02	0·00	0·06	0·06	0·05	0·00	0·12	0·12	0·02
MgO	15·24	15·32	12·36	12·30	15·05	15·03	13·12	17·27	17·11	15·77	12·58	15·01	15·68	10·14	14·57	15·42	16·24	10·80
CaO	11·45	12·17	12·37	12·21	11·49	12·15	11·75	12·53	12·62	10·11	11·70	12·29	12·48	11·20	10·58	12·06	11·66	12·21
Na_2O	0·96	0·76	0·10	0·11	0·96	0·82	0·98	0·83	0·79	0·77	1·12	1·03	0·75	2·31	1·53	0·93	0·47	1·71
K_2O	0·13	0·22	0·03	0·07	0·18	0·16	0·19	0·09	0·13	0·07	0·13	0·15	0·09	0·06	0·21	0·19	0·07	0·34
Total	96·05	96·42	96·51	97·10	96·47	96·57	96·12	97·15	97·21	95·97	96·30	97·88	98·02	97·23	97·66	97·73	97·47	96·71
Si	7·251	7·377	7·835	7·860	7·215	7·294	7·203	7·352	7·355	7·325	7·045	7·286	7·428	6·465	6·996	7·145	7·663	6·350
Ti	0·014	0·014	0·016	0·002	0·015	0·018	0·031	0·015	0·028	0·015	0·017	0·027	0·047	0·018	0·031	0·026	0·006	0·032
Al^{IV}	0·749	0·623	0·165	0·140	0·785	0·706	0·797	0·648	0·645	0·675	0·955	0·714	0·572	1·535	1·004	0·855	0·337	1·650
Al^{VI}	0·505	0·433	0·095	0·117	0·473	0·417	0·571	0·394	0·399	0·439	0·505	0·433	0·366	0·726	0·519	0·517	0·254	0·977
Fe^{3+}	0·194	0·071	0·032	0·057	0·227	0·119	0·082	0·091	0·055	0·463	0·196	0·078	0·043	0·275	0·380	0·168	0·201	0·094
Fe^{2+}	1·317	1·297	2·111	2·172	1·420	1·389	1·564	0·987	0·973	1·501	1·847	1·379	1·270	2·210	1·617	1·280	1·421	1·662
Mg	3·307	3·311	2·745	2·716	3·269	3·260	2·877	3·665	3·627	3·431	2·790	3·212	3·330	2·274	3·154	3·294	3·471	2·389
Mn	0·006	0·000	0·057	0·041	0·017	0·012	0·009	0·005	0·011	0·011	0·008	0·009	0·011	0·000	0·007	0·012	0·006	0·009
Ca	1·763	1·881	1·970	1·931	1·767	1·879	1·842	1·899	1·916	1·533	1·841	1·881	1·899	1·773	1·605	1·831	1·767	1·929
Na	0·267	0·213	0·029	0·031	0·267	0·230	0·278	0·228	0·217	0·211	0·319	0·285	0·207	0·662	0·420	0·256	0·129	0·489
K	0·024	0·040	0·006	0·013	0·033	0·029	0·035	0·016	0·023	0·013	0·024	0·027	0·016	0·011	0·038	0·034	0·013	0·064
Sum	15·397	15·261	15·061	15·081	15·489	15·354	15·289	15·299	15·250	15·617	15·547	15·331	15·189	15·950	15·770	15·419	15·268	15·645

Table 5: Whole-rock compositions of eclogites from East Kunlun Orogen

Sample:	16KL-13	KL-14	KL-15	KL-16	KL-20	KL-23	KL-24	KL-26	KL-27	KL-37	KL-38	KL-40	KL-43	KL-44
Location:	Hekete	Hekete	Hekete	Hekete	Hekete	Hekete	Hekete	Hekete	Hekete	Hekete	Hekete	Hekete	Hekete	Hekete
Major elements (wt %)														
SiO_2	47·22	46·87	46·72	50·59	47·21	46·80	47·09	46·85	48·59	49·28	50·90	49·09	48·27	46·01
TiO_2	3·47	2·43	1·47	2·01	2·86	2·71	2·81	3·97	1·83	1·79	1·70	2·08	2·35	2·54
Al_2O_3	13·40	14·49	16·78	15·03	12·66	13·91	13·58	12·87	14·52	14·20	13·81	14·38	13·89	14·13
TFe_2O_3	16·60	15·36	12·84	13·16	16·13	18·30	18·39	14·88	14·30	13·82	13·51	15·16	15·74	17·27
MnO	0·23	0·21	0·18	0·17	0·22	0·27	0·27	0·16	0·19	0·19	0·18	0·21	0·21	0·27
MgO	5·61	6·54	8·06	6·64	6·04	5·87	5·74	7·58	7·13	7·27	6·81	6·82	7·04	7·08
CaO	8·97	9·87	11·73	9·17	10·99	9·66	9·73	9·93	9·94	10·07	9·58	9·38	9·11	9·51
Na_2O	2·26	2·20	1·63	1·47	2·06	1·99	1·88	2·76	2·21	2·17	2·00	1·97	1·27	1·91
K_2O	0·53	0·80	0·16	0·26	0·70	0·39	0·27	0·11	0·53	0·41	0·38	0·20	0·63	0·53
P_2O_5	0·44	0·28	0·06	0·50	0·30	0·27	0·31	0·32	0·14	0·12	0·14	0·21	0·20	0·25
LOI	0·62	0·54	0·29	0·24	0·69	0·05	0·06	0·48	0·46	0·39	0·33	0·22	1·03	0·58
Total	99·34	99·60	99·94	99·25	99·87	100·11	100·02	99·91	99·85	99·71	99·36	99·73	99·74	100·08
Trace elements (ppm)														
Li	9·572	11·886	12·266	10·178	3·894	7·328	6·108	22·46	21·34	11·988	12·776	28·92	16·782	26·5
Sc	35·2	36·18	37·06	23·12	35·86	40·32	40·38	28·88	34·8	35·62	32·74	35·6	33·48	34·48
V	420·2	366·8	242·8	199·3	437·8	389·4	383·2	528·2	277·4	306·4	282·6	284	284·4	315
Cr	71·32	68·9	194	97·32	146·88	30·7	33·98	54·82	141	156·1	139·8	128·42	116·98	98·24
Co	49·3	50·16	43·92	45·36	48·48	48·44	55·64	38·26	55·22	51·12	48·26	45·26	57·38	44·88
Ni	41·4	45·08	53·2	52·26	67·96	24·36	37·46	38·7	81·76	80·58	86·46	57·9	90·3	60·34
Cu	44·76	49·46	22·68	2·888	93·5	64·82	67·44	15·508	96·14	74·52	76·84	47·94	73·08	61·32
Zn	102·78	96·9	66·14	106·9	107·38	107·76	109·48	73·1	86·96	90·9	85·8	80·48	96·64	99·38
Ga	22·5	21·18	16·002	28·04	22·04	21·00	20·44	29·26	19·05	18·99	17·586	17·872	18·384	18·98
Rb	22·02	28·4	6·744	8·066	15·188	17·08	11·748	4·922	23·24	14·978	12·254	6·686	31·72	26·92
Sr	165·48	192·16	110·96	124·38	386	205·2	212·4	326·2	162·2	134·84	125·42	138·2	137·1	130·72
Y	42·06	35·9	24·74	22·3	35·64	39·2	39·76	24·44	27·38	26·18	25·18	30·94	35·44	35·2
Zr	199·75	141·03	93·59	106·95	100·74	164·44	187·17	180·54	105·37	92·21	95·23	111·08	140·79	148·73
Nb	34·68	26·03	9·71	18·38	18·79	21·98	22·23	34·49	12·64	11·27	10·64	13·52	17·01	15·70
Cs	1·375	1·088	0·158	0·786	0·835	0·754	0·499	0·227	1·255	1·550	1·379	0·750	2·662	0·399
Ba	62·72	83·78	17·51	41·6	207·8	40·48	37·96	13·422	57·68	67·4	62·26	30·02	45·5	55·14
La	26·38	19·054	3·776	14·356	17·228	9·786	14·94	18·414	8·91	7·704	8·266	11·246	12·09	13·884
Ce	55·86	40·82	8·954	30·78	40·28	21·36	33·08	38·84	20·08	17·132	17·986	25·48	26·56	31·16
Pr	7·496	5·542	1·3392	4·258	5·888	3·138	4·662	5·316	2·914	2·47	2·53	3·608	3·754	4·43
Nd	32·68	24·28	6·874	19·092	27·06	15·296	21·5	23·52	13·63	11·78	11·886	16·594	17·056	20·24
Sm	7·578	5·966	2·61	4·584	7·006	4·946	5·992	5·704	3·848	3·63	3·556	4·388	4·716	5·346
Eu	2·432	1·881	1·122	1·562	2·460	1·850	2·056	2·272	1·458	1·416	1·388	1·556	1·666	1·874
Gd	8·028	6·520	3·732	4·798	7·470	6·596	7·110	5·628	4·636	4·502	4·448	5·110	5·734	6·274
Tb	1·297	1·079	0·685	0·749	1·196	1·172	1·210	0·852	0·796	0·771	0·760	0·881	1·017	1·053
Dy	8·140	6·882	4·638	4·562	7·302	7·548	7·732	4·982	5·144	4·932	4·866	5·776	6·604	6·608
Ho	1·661	1·396	0·983	0·899	1·419	1·548	1·572	0·962	1·058	1·013	0·995	1·194	1·351	1·333
Er	4·596	3·876	2·808	2·444	3·824	4·274	4·360	2·590	2·958	2·804	2·754	3·332	3·804	3·690
Tm	0·640	0·546	0·402	0·339	0·515	0·598	0·608	0·353	0·413	0·393	0·385	0·465	0·534	0·512
Yb	4·072	3·444	2·602	2·126	3·152	3·762	3·852	2·250	2·616	2·472	2·436	2·940	3·344	3·208
Lu	0·599	0·499	0·389	0·307	0·453	0·555	0·569	0·335	0·385	0·366	0·363	0·437	0·497	0·473
Hf	4·822	3·698	2·402	2·673	2·730	4·085	4·668	4·307	2·650	2·339	2·447	2·749	3·440	3·587
Ta	2·096	1·637	0·604	1·143	1·161	1·308	1·334	2·121	0·840	0·646	0·617	0·779	1·000	0·939
Pb	2·380	11·698	10·046	12·590	11·400	10·740	10·700	4·966	10·204	5·130	3·214	6·572	7·828	9·052
Th	2·396	1·733	0·312	1·512	2·372	1·647	1·784	1·746	0·927	1·016	1·124	1·545	1·642	1·634
U	0·727	0·637	0·487	0·505	1·225	1·084	1·275	0·624	0·351	0·324	0·320	0·389	0·677	0·454

(continued)

Table 5: Continued

Sample:	16KL-52	KL-53	KL-54	KL-56	KL-64	KL-80	KL-81	KL-83	KL-84	KL-91	KL-92
Location:	Xiarihamu	Xiarihamu	Xiarihamu	Xiarihamu	Xiarihamu	Xiarihamu	Xiarihamu	Xiarihamu	Xiarihamu	Xiarihamu	Xiarihamu
Major elements (wt %)											
SiO_2	45·75	50·53	50·19	48·99	50·50	50·88	51·63	51·81	51·00	46·11	45·18
TiO_2	6·27	1·18	1·24	1·42	1·02	0·82	1·04	1·62	1·04	2·94	3·04
Al_2O_3	12·32	12·71	13·46	13·59	13·12	12·85	12·63	12·45	12·62	13·39	12·69
TFe_2O_3	15·85	12·74	12·14	14·40	11·91	10·78	11·59	14·19	12·16	17·49	18·20
MnO	0·22	0·18	0·17	0·20	0·17	0·20	0·17	0·23	0·23	0·21	0·21
MgO	6·56	7·23	7·90	6·92	8·18	8·31	7·98	6·16	7·63	6·49	6·92
CaO	9·78	10·88	11·67	11·12	11·04	10·50	10·23	9·98	11·75	10·76	11·11
Na_2O	2·70	2·46	1·57	2·12	1·93	2·37	2·11	2·26	1·71	2·03	2·15
K_2O	0·08	0·52	0·28	0·22	0·34	0·50	0·26	0·18	0·19	0·11	0·11
P_2O_5	0·22	0·09	0·09	0·11	0·09	0·06	0·07	0·13	0·08	0·25	0·26
LOI	0·04	0·57	0·52	0·35	0·83	1·80	1·25	0·09	0·60	0·09	0·11
Total	99·79	99·09	99·22	99·45	99·13	99·08	98·95	99·02	99·01	99·86	99·99
Trace elements (ppm)											
Li	19·44	22·24	15·276	20·6	13·855	24·76	24·62	16·776	55·04	12·12	11·144
Sc	45·38	39·08	37·28	42·3	38·006	36·18	36·4	38·34	35·68	38·86	42·26
V	674·4	336·8	316·6	370·6	309·467	263·4	308·8	365·6	302	455·8	494·4
Cr	48·2	160·14	215·4	173·9	240·3	334·6	348·8	94·82	337·6	2·038	5·848
Co	46·44	44·98	46·06	57·22	46·691	42·22	43·32	45·28	45·34	51·54	54·38
Ni	35·2	69·8	94·64	84·72	97·653	110·64	126·16	70·74	124·84	4·48	6·642
Cu	65·66	77·86	75·82	194·26	88·127	31·52	69·86	169·92	91·46	42·8	49·38
Zn	84·56	76·3	70·8	78·72	74·589	70·1	74·36	81·68	66·92	89·94	92·26
Ga	18·862	15·562	15·586	16·292	15·152	13·65	14·518	15·392	12·792	16·952	17·81
Rb	3·098	12·226	8·616	8·544	14·571	21·9	7·682	3·848	5·186	2·002	1·0938
Sr	65·48	229·4	152·82	170·12	164·9	261·4	210·2	134	141·7	382	344·8
Y	42·26	20·96	19·976	24·8	18·359	15·078	17·646	30·42	17·688	14·978	15·802
Zr	169·17	64·14	62·23	74·21	47·49	35·55	49·08	92·63	48·60	84·45	88·93
Nb	32·60	3·67	5·56	6·44	2·94	2·35	3·67	9·68	3·00	8·94	9·64
Cs	0·615	2·216	1·5434	0·7876	0·602	1·2818	0·9232	0·278	0·691	0·345	0·245
Ba	10·826	212·4	45·3	42·16	66·105	99·92	58·96	77·140	27·220	17·066	11·088
La	11·314	3·796	4·912	6·04	4·003	3·596	3·064	7·746	3·018	7·808	7·788
Ce	25·34	9·408	11·384	13·836	8·865	7·296	7·426	17·332	7·570	17·588	17·916
Pr	3·742	1·485	1·7252	2·056	1·321	1·077	1·187	2·520	1·211	2·558	2·618
Nd	17·958	7·498	8·308	9·960	6·504	5·216	6·018	11·776	6·140	11·804	12·158
Sm	5·08	2·408	2·482	2·936	2·060	1·612	1·9178	3·448	1·958	2·812	2·946
Eu	1·565	0·919	0·899	1·079	0·753	0·619	0·731	1·181	0·718	1·138	1·144
Gd	6·004	3·122	3·006	3·672	2·615	2·104	2·452	4·332	2·456	2·982	3·134
Tb	1·078	0·559	0·535	0·653	0·482	0·386	0·444	0·777	0·448	0·462	0·493
Dy	7·510	3·742	3·560	4·414	3·233	2·602	3·068	5·242	3·016	2·852	3·040
Ho	1·639	0·796	0·747	0·945	0·680	0·563	0·667	1·127	0·650	0·574	0·613
Er	4·752	2·286	2·126	2·706	1·938	1·658	1·939	3·284	1·879	1·557	1·646
Tm	0·689	0·324	0·300	0·390	0·276	0·239	0·276	0·468	0·268	0·205	0·218
Yb	4·474	2·084	1·919	2·506	1·780	1·584	1·802	3·010	1·728	1·246	1·334
Lu	0·670	0·311	0·282	0·372	0·270	0·238	0·267	0·446	0·260	0·178	0·192
Hf	4·135	1·524	1·484	1·770	1·144	0·844	1·161	2·186	1·137	2·611	2·718
Ta	1·736	0·217	0·376	0·670	0·179	0·138	0·549	0·532	0·176	0·535	0·528
Pb	1·176	4·966	1·944	2·964	4·503	1·712	1·565	0·838	0·704	0·579	0·446
Th	0·931	0·457	0·637	0·693	0·407	0·282	0·340	0·972	0·337	0·114	0·128
U	0·199	0·283	0·291	0·363	0·204	0·095	0·124	0·314	0·113	0·112	0·033

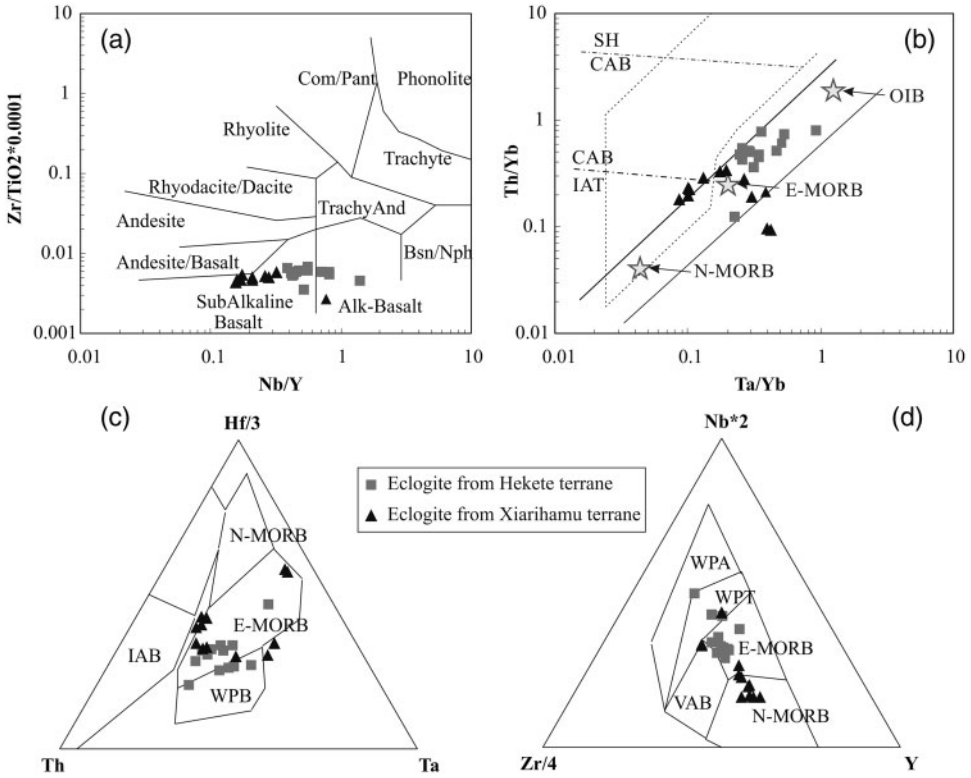

Fig. 4. Discrimination diagrams for eclogites from the EKO. (a) Nb/Y vs Zr/Ti after Winchester & Floyd (1976) for rock classification. (b) Ta/Yb vs Th/Yb (modified after Pearce, 1982). The compositions of modern normal mid-ocean ridge basalts (N-MORB), enriched mid-ocean ridge basalts (E-MORB), and ocean-island basalts (OIB) are from Sun & McDonough (1989); (c) Hf–Th–Ta discrimination diagram of Wood (1980). (d) Nb–Zr–Y discrimination diagram of Meschede (1986).

chemical zoning; the X_{Mn} [= Mn/(Fe + Mg + Ca + Mn)] values decrease slightly from core to rim and X_{Mg} [= Mg/(Fe + Mg + Ca + Mn)] exhibits reversed zoning. Omphacite in eclogites from the Kehete and Wenquan terranes have higher jadeite contents than that from the Xiarihamu terrane (Table 2, Fig. 3b). Phengite is a minor phase found only in the eclogites from the Kehete terrane. Si contents in phengite vary from 3·44 to 3·59 Si atoms per formula unit (a.p.f.u.) based on 11 oxygens (Table 3).

Amphibole is a retrograde phase in eclogites from all the three terranes. Hbl + Pl occurs as a symplectite or symplectitic coronas after garnet and omphacite (Fig. 2g and i). Results of EPMA (Fig. 3c, Table 4) indicate that they show wide compositional variations, but there is no significant difference between coronas and coarse amphibole grains in the matrix.

Twenty-six eclogite samples (14 from the Kehete terrane in the east and 12 from the Xiarihamu terrane in the west) were selected for whole-rock compositional analysis at the China University of Geosciences, Beijing (Table 5). All eclogite samples are predominantly basaltic with SiO_2 (46·01–51·0 wt %), TiO_2 (0·84–6·27 wt %), MgO (5·61–8·31 wt %), CaO (8·97–11·73 wt %) and Na_2O (1·27–2·70 wt %). In a (Nb/Y) vs (Zr/TiO_2) diagram (Winchester & Floyd, 1976), five samples plot in the alkaline field, whereas others plot in the subalkaline field (Fig. 4a). Discrimination diagrams, as well as trace element patterns, show that the eclogites from the Kehete terrane have the geochemical characteristics of enriched mid-ocean ridge basalts (E-MORB) to ocean-island basalts (OIB) or within-plate basalts (WPB), whereas eclogites from the Xiarihamu terrane are similar to E-MORB and N-MORB (Figs 4b–d and 5). The geochemical characteristics of these eclogites suggest that their protoliths were oceanic crust (including seamount) basalts.

METAMORPHIC *P–T* PATHS

Three stages of metamorphism of eclogites in the East Kunlun can be identified: peak stage I, with a mineral assemblage of garnet + Omp + Coe/Qtz + Rutile ± Phengite; stage II, decompression of omphacite at dry conditions to Cpx2 + oligoclase; stage III, amphibolite overprinting with addition of H_2O in the mid-crust. Coesite pseudomorphs and quartz exsolution rods in Omp suggest UHP conditions during the peak stage of metamorphism. Grt–Opm–Phn geothermobarometry (Krogh Ravna & Terry, 2004) also indicates UHP conditions of $P = 2{\cdot}91$–$3{\cdot}03$ GPa and $T = 610$–675°C (Fig. 6). The *P–T* conditions of omphacite decompression into Cpx2 + oligoclase cannot be precisely determined, but should lie below the stability curve of Jadeite + Quartz = Albite. The amphibolite-facies retrogression is marked by varying degrees of amphibolitization in all

eclogite blocks with the retrograde assemblage Hbl + Ep + Pl at ~600°C and 0·6 GPa. Therefore, eclogites from the EKO record a clockwise *P–T* path from subduction to exhumation (Fig. 7).

HP–UHP METAMORPHIC AGES

Three eclogites and two garnet–mica schist samples (three from the Kehete terrane and two from the Xiarihamu terrane) were selected for zircon U–Pb dating (Supplementary Data Appendix Tables S1 and S2; supplementary data are available for downloading at http://www.petrology.oxfordjournals.org).

Zircons separated from the eclogite blocks (samples 16KL13 and 16KL27 from Kehete and 16KL87 from Xiarihamu) are round to ovoid crystals and have a diameter of ~50–150 μm. They all show a typical metamorphic origin with oval shapes and fir-tree and radial sector zoning in CL images (Fig. 8). Garnet + omphacite + rutile inclusions were identified by Raman

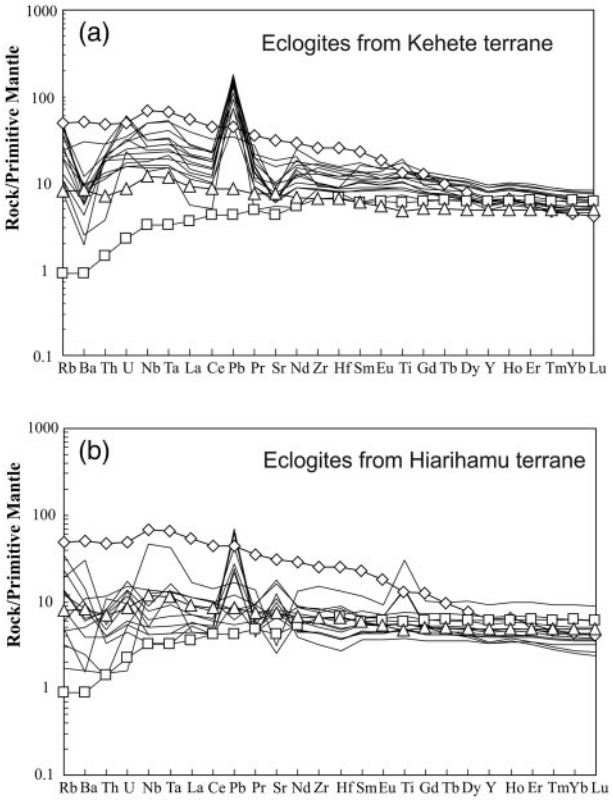

Fig. 5. Primitive mantle-normalized multi-element patterns for eclogites from the Kehete terrane (a) and the Xiarihamu terrane (b). Normalization values are from Sun & McDonough (1989).

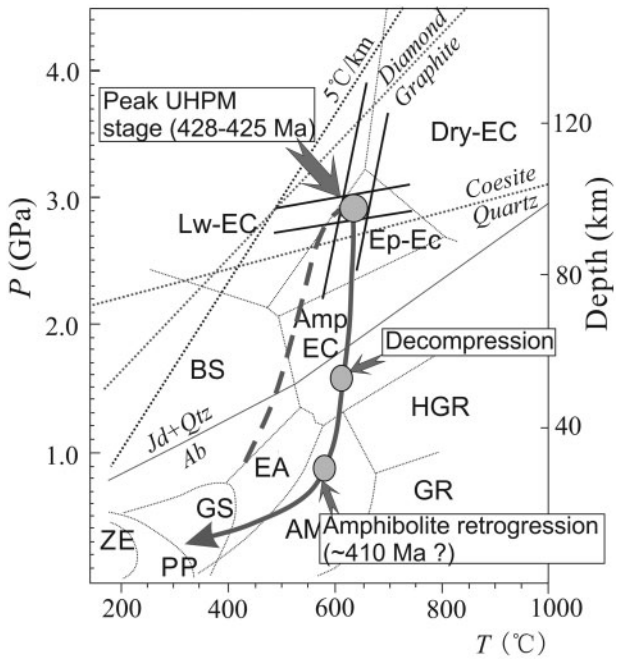

Fig. 7. *P–T–t* path of eclogites in the EKO. ZE, zeolite facies; PP, prehnite–pumpellyite facies; EA, epidote amphibolite facies; AM, amphibolite facies; GR, granulite facies; HGR, high-pressure granulite facies; BS, blueschist facies; Amp EC, amphibole eclogite facies; Ep-EC, epidote eclogite facies; Lw-EC, lawsonite eclogite facies (after Liou *et al.*, 1998).

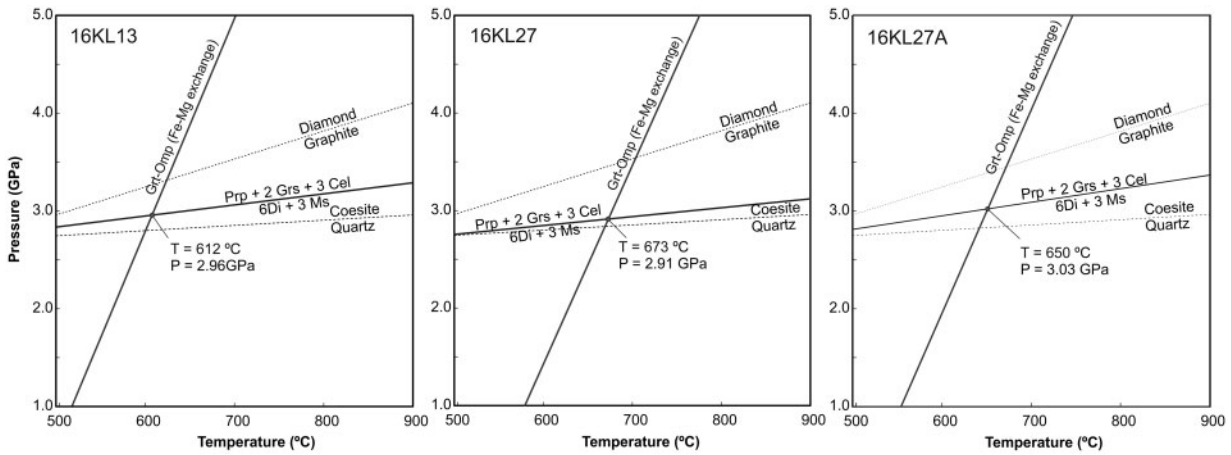

Fig. 6. *P–T* diagrams for three eclogite samples from the Hekete terrane with the assemblage Grt + Omp + Phn. Calculation was performed using 'P-T calc eclogite' of Krogh Ravna & Terry (2004).

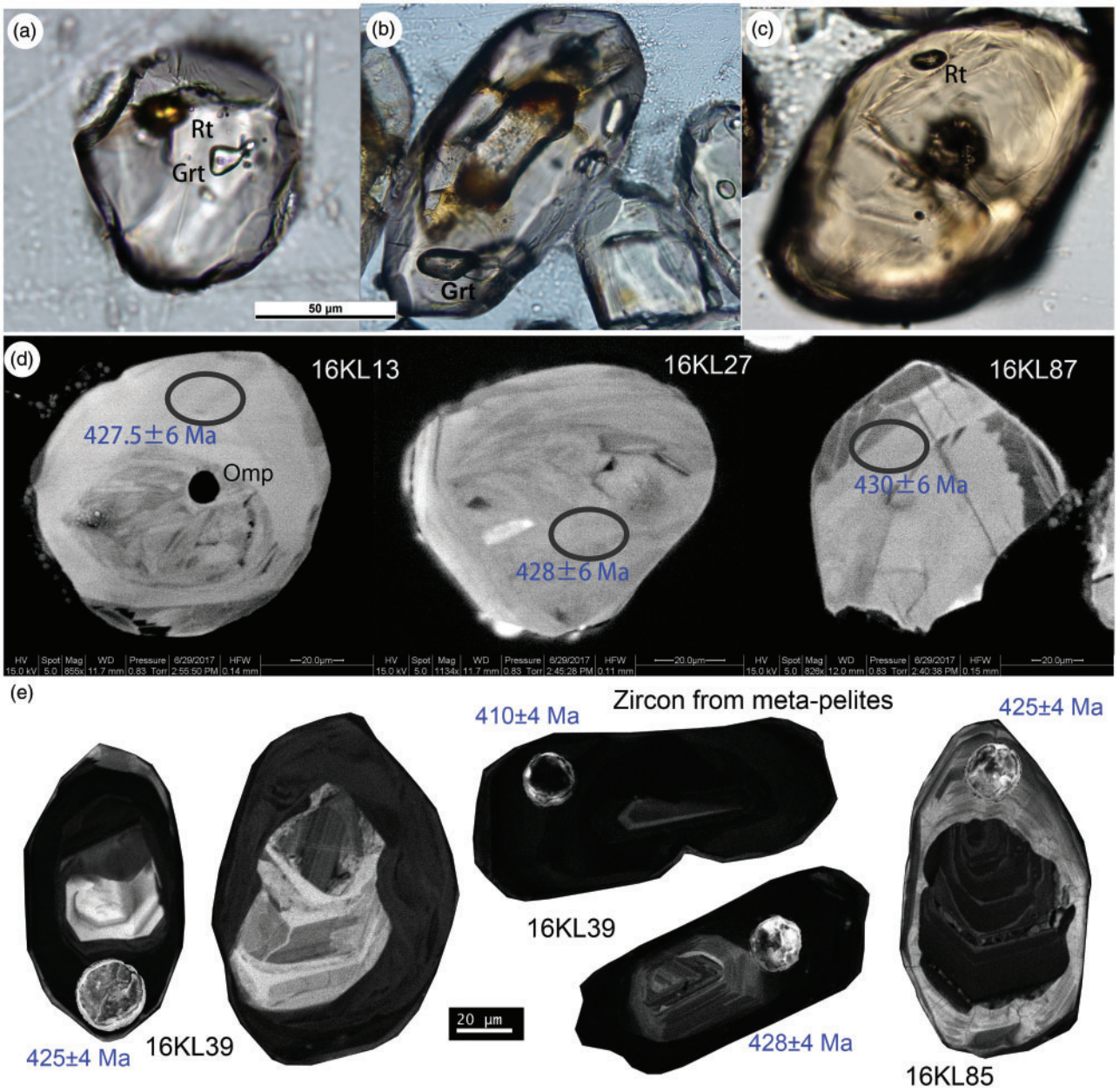

Fig. 8. Photomicrographs and cathodoluminescence (CL) images of zircons from the eclogites and metapelites in the EKO. (a) Garnet and rutile inclusions in zircon from eclogite (16KL27). (b) Garnet inclusion in the rim domain of zircon from metapelite (16KL39). (c) Rutile inclusions in zircon from metapelite (16KL39). (d) CL images of zircons from eclogites; omphacite (Omp) inclusion should be noted. (e) CL images of zircons from metapelites. The core–rim structure and dark luminance of the rim domains should be noted.

spectroscopy (Fig. 8a and b). The U content in zircon varies from 220 to 1487 ppm (mostly 300–600 ppm), with Th/U ratios of 0·02–0·43. Thirty-two analyses of 16KL13 yield a concordia age of 427·5 ± 2·1 Ma (MSWD = 0·36); 30 analyses of 16KL27 yield a concordia age of 425·5 ± 2·2 Ma (MSWD = 0·069), and 30 analyses of 16KL87, 427·7 ± 2·2 Ma (MSWD = 0·53) (Fig. 9). These ages suggest that the eclogites in the East Kunlun formed in a narrow age range of 428–425 Ma, the same as eclogites (428 ± 2 Ma) from the Wenquan Terrane in the easternmost EKO (Meng *et al.*, 2013).

Zircons in the two metapelitic samples (garnet–mica schists) (16KL39 from the east section and 16KL85 from the west section) show clear internal zoning with inherited detrital cores and metamorphic rims (Fig. 8). Garnet and rutile inclusions were detected in the metamorphic rims by Raman spectroscopy (Fig. 8b and c). In sample 16KL39 from the east section of the East Kunlun eclogite belt, a total of 77 zircon grains were analyzed, and 61 core analyses yielded $^{206}Pb/^{238}U$ ages varying from 453 ± 5 to 971 ± 10 Ma, with peaks at 465, 512, 603, 712, 834 and 923 Ma. Sixteen zircon rims in sample

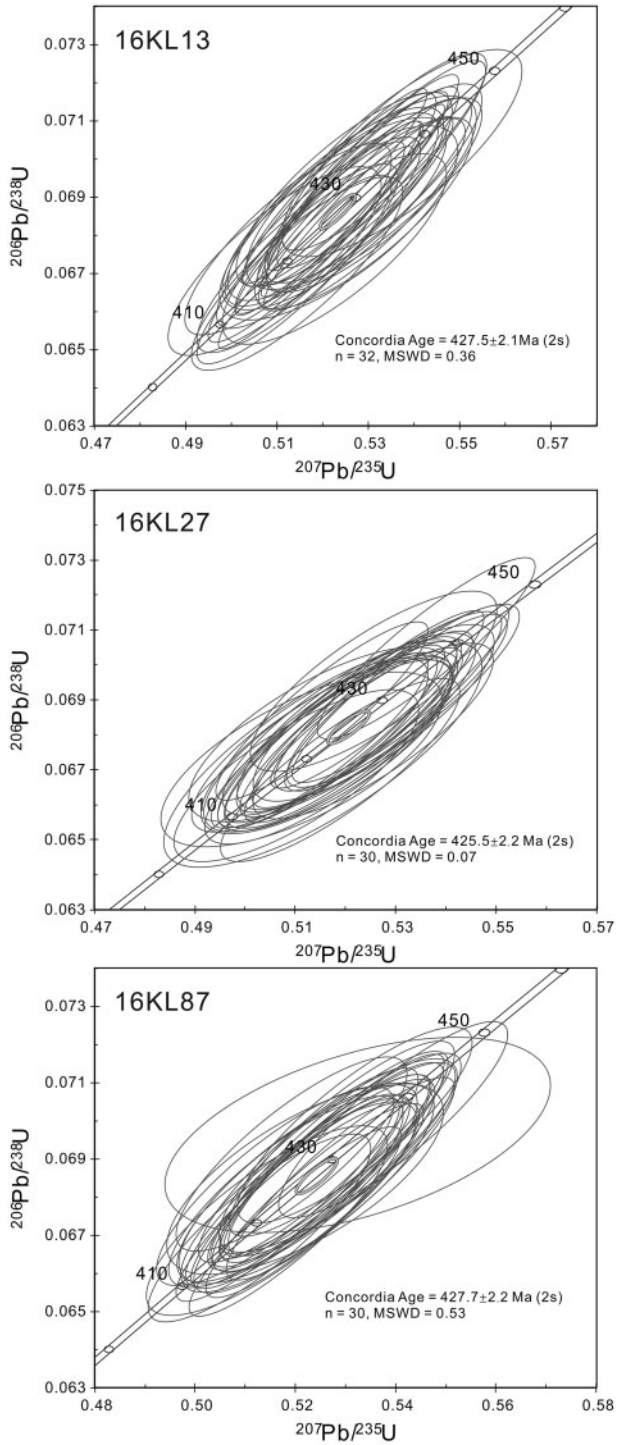

Fig. 9. Concordia diagrams for eclogites in the EKO.

16KL39 have significantly low Th/U ratios (0·01–0·06). Twelve analyses form a concordia age of 427·3 ± 1·4 Ma (MSWD = 0·10) (Fig. 10a–c), which is consistent with the metamorphic ages of the eclogites. Another four analyses gave a younger mean age of 410·5 ± 2 Ma (MSWD = 0·05), which may represent the amphibolite-facies retrograde age of the HP belt. Forty-five analyses of zircon cores from sample 16KL85 yielded similar ages, ranging from 469 to 1162 Ma. Six analyses of zircon rims gave a concordia age of 427·5 ± 2 Ma (MSWD = 0·09) (Fig. 10d–f), the same as the ages of the eclogites.

DISCUSSION

The conditions of UHP metamorphism in the East Kunlun Orogen

The 500 km long eclogite belt indicates the existence of HP–UHP metamorphism in a subduction zone associated with the East Kunlun Orogen. Its rock assemblage, together with ophiolite and arc-volcanic rocks along this belt, suggests a tectonic mélange and accretionary complex that combines oceanic subduction and continental collision. Peak metamorphic conditions are within the coesite stability field, evidenced by quartz exsolution rods in Omp, coesite pseudomorphs in garnet and omphacite, and *P–T* calculations using the Grt–Omp–Phn geothermobarometer of Krogh Ravna & Terry (2004). The metamorphic *P–T–t* path of the eclogite shows a clockwise decompression path, suggesting that the eclogite blocks were exhumed from depths of 100–120 km.

Evolution of the Proto-Tethys Ocean and formation of the Pan-North-China Continent

The remnants of the Early Paleozoic Qinling–Qilian–Kunlun Ocean preserved in the present-day Chinese continent represent part of the Proto-Tethys Ocean (Mattern & Schneider, 2000; von Raumer & Stampfli, 2008; Stampfli *et al.*, 2013). All blocks in this region, including the South Kunlun Block, Qaidam–Quangji Block, Central Qilian Block, South China Block and North Qilian Block, which have been referred to as peri-Gondwana, have similar Precambrian basements (records of 1·2–0·9 Ga orogenic assembly and 0·85–0·7 Ga rifting of Rodinia). They are believed to have dispersed from East Gondwanaland during breakup of the Rodinia supercontinent (Yin & Harrison, 2000; Gehrels *et al.*, 2003; Cawood *et al.*, 2007, 2013; von Raumer & Stampfli, 2008; Song *et al.*, 2012, 2014; Han *et al.*, 2016; Xu *et al.*, 2016), in the late Neoproterozoic, as recorded by the ~600–580 Ma rift-related volcano-sedimentary sequence and the oldest ophiolite (550 Ma) in the Qilian orogen (Song *et al.*, 2013; Xu *et al.*, 2015).

The remnants of the Proto-Tethys Ocean preserved in the northern Tibetan Plateau can be divided into the Qilian Ocean in the north and the East Kunlun Ocean in the south, separated by the Qaidam Block. Subparallel oceanic-type accretionary belts and continental-type collisional zones, together with the three HP and UHP metamorphic belts (Fig. 1), suggest that the Proto-Tethys Ocean must have experienced an evolution from initial subduction at ~520 Ma to final closure at ~410 Ma. The Qilian Ocean between the NCC–Tarim and Qaidam blocks started to subduct at ~520 Ma and closed at ~440 Ma, followed by the northward continental subduction–collision of the Qaidam block at

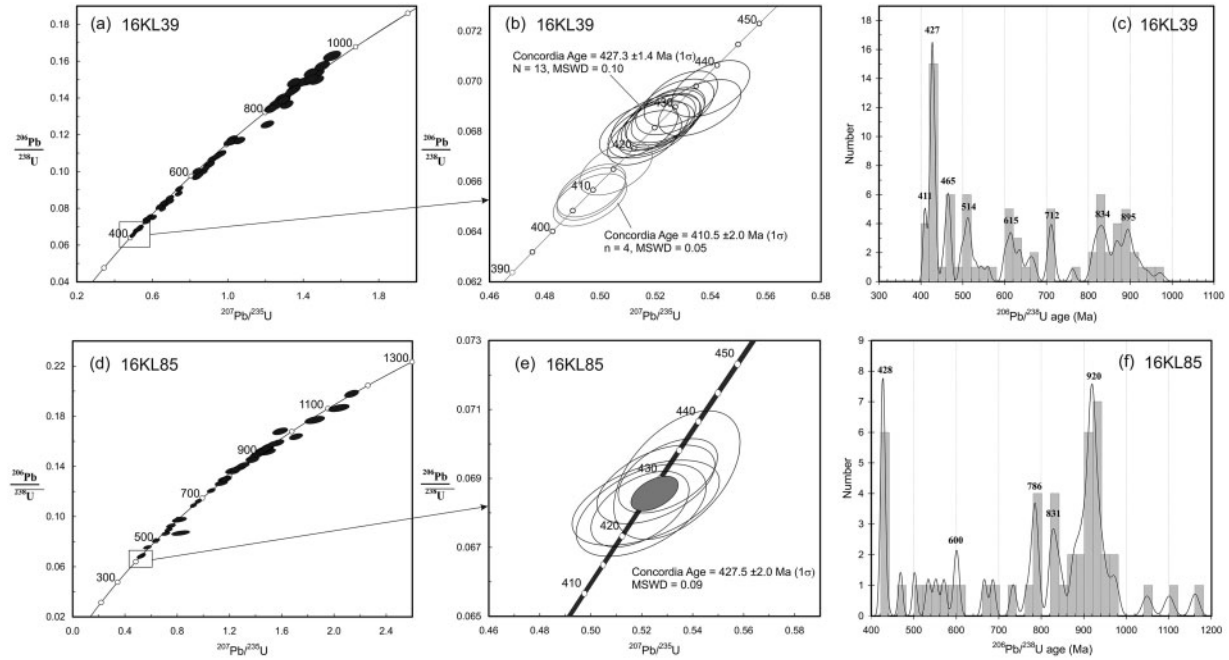

Fig. 10. Concordia and histograms showing the age distribution of detrital zircons from two metapelite samples in the EKO. Sample 16KL39 is from the Kehete terrane, and 16KL85 is from the Xiarihamu terrane.

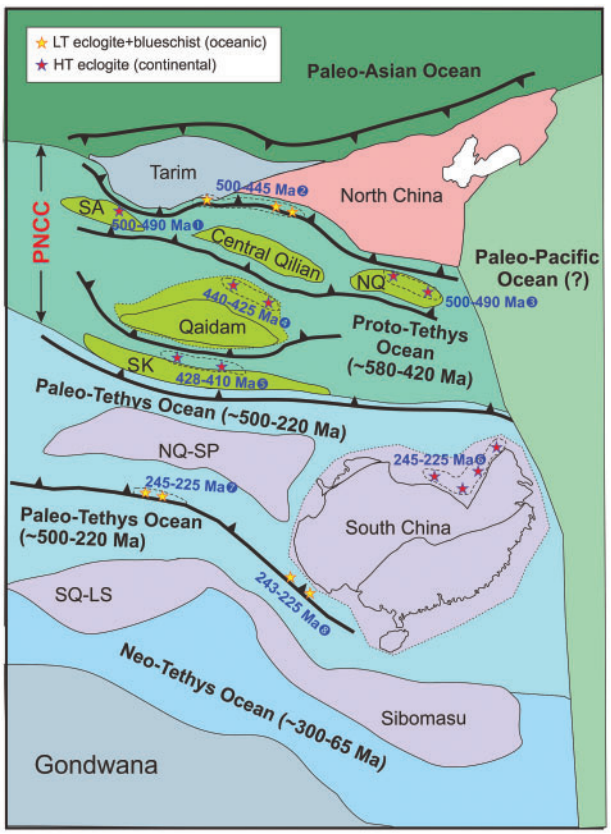

Fig. 11. Schematic illustration of the evolution from the Proto-Tethys to the Neo-Tethys oceans and the formation of the Pan-North-China Continent (PNCC). 1, UHP metamorphic ages of South Altun (Liu *et al.*, 2012). 2, HP metamorphic ages of eclogite and blueschist of North Qilian (Song *et al.*, 2006; Zhang *et al.*, 2007). 3, UHP metamorphic ages of North Qinling (Liu *et al.*, 2016). 4, UHP metamorphic ages of North Qaidam (Song *et al.*, 2014). 5, HP–UHP metamorphic ages of East Kunlun (Meng *et al.*, 2013; Qi *et al.*, 2014; this study). 6, UHP metamorphic ages of Dabie–Sulu (Li *et al.*, 1993; Liu *et al.*, 2006). 7, HP metamorphic ages of eclogite and blueschist of North Qiangtang (Zhai *et al.*, 2011). 8, HP metamorphic ages of blueschists in Lanchangjiang (Wang *et al.*, in press). SA, South Altun; QL, Qilian Block; NQ, North Qinling; SK, South Kunlun; NQ-SP, North Qiangtang–Songpan; SQ-LS, South Qiangtang–Lhasa.

~440–420 Ma (Song *et al.*, 2013, 2014). Ophiolites in the EKO record formation ages of 540–460 Ma (e.g. Yang *et al.*, 1996; Meng *et al.*, 2015; Qi *et al.*, 2016; Li *et al.*, 2017), suggesting that the Kunlun Ocean between the Qaidam and South Kunlun blocks had a similar history to the Qilian Ocean in the north. Arc volcanic rocks suggest that the East Kunlun Ocean may have started subduction at ~450 Ma. Ages of the Kunlun UP–UHP belt reveal that the Proto-Tethys Ocean finally closed at ~428–410 Ma, resulting in the formation of a united continent in North China by the end of Early Paleozoic, named 'the Pan-North-China Continent'.

Transition from Proto-Tethys to Paleo-Tethys in the Northern Tibetan Plateau

The Proto-Tethys Ocean is generally considered to have initiated at ~550 Ma between the continents of Laurasia and Gondwana (von Raumer & Stampfli, 2008; Song *et al.*, 2013). However, the transition from Proto-Tethys to Paleo-Tethys is always ambiguous because there is no clear subdivision of these two periods of oceanic spreading. As shown in Fig. 11, after closure of the Proto-Tethys Ocean at ~420–410 Ma in the East Kunlun

orogen, a wide Paleo-Tethys Ocean, which was named the 'Rheic Ocean' by von Raumer & Stampfli (2008), developed in the Late Paleozoic in the south and east between Gondwana and the Pan-North-China Continent (or Hunic terranes; von Raumer *et al.*, 2003). Ophiolites in the A'nyemaqen accretionary belt of the East Kunlan (e.g. Yang *et al.*, 1996; Bian *et al.*, 2004) and in Central Qiangtang (Zhai *et al.*, 2016) suggest that the oceanic crust of the Paleo-Tethys Ocean could be as old as 500 Ma. The Paleo-Tethys Ocean had closed by ~220 Ma, marked by collision between the South China and North China blocks in the north (e.g. Li *et al.*, 1993; Liu *et al.*, 2006) and between the South Qiangtang–Sibomasu blocks and South China–North Qiangtang blocks in the south (Zhai *et al.*, 2011; Wang *et al.*, 2018) (Fig. 11).

CONCLUSIONS

(1) The eclogite belt consists of eclogite blocks, metapelites, marble and minor serpentinite blocks, and extends laterally for ~500 km within the Kunlun orogenic belt. All eclogites show geochemical characteristics with E-MORB and OIB affinities.

(2) Coesite pseudomorphs, quartz exsolution in omphacite, and *P–T* calculations reveal that the East Kunlun eclogites experienced UHP metamorphism at conditions of 29–30 kbar and 610–675°C. Zircon U–Pb analyses show they formed at 430–410 Ma.

(3) The East Kunlun eclogite belt was produced in response to final closure of the Proto-Tethys Ocean at the end of the Early Paleozoic.

ACKNOWLEDGEMENTS

We thank Xianhua Li and his group for help with the secondary ion mass spectrometry U–Pb dating of zircons, and Xiaoli Li for help with electron microprobe analysis. We also thank Hannes Brueckner, Gueltekin Topuz and an anonymous reviewer, as well as Editor Alasdair Skelton, for their constructive comments, which significantly improved the quality of the paper.

FUNDING

This research was financially supported by the Major State Basic Research Development Program (2015CB856105) and the National Natural Science Foundation of China (grants 41572040 and 41372060).

SUPPLEMENTARY DATA

Supplementary data for this paper are available at *Journal of Petrology* online.

REFERENCES

Agard, P., Yamato, P., Jolivet, L. & Burov, E. (2009). Exhumation of oceanic blueschists and eclogites in subduction zones: timing and mechanisms. *Earth-Science Reviews* **92**, 53–79.

Andersen, T. (2002). Correction of common lead in U-Pb analyses that do not report ^{204}Pb. *Chemical Geology* **192**, 59–79.

Bian, Q.-T., Li, D.-H., Pospelov, I., Yin, L.-M., Li, H.-S., Zhao, D.-S., Chang, C.-F., Luo, X.-Q., Gao, S.-L., Astrakhantsev, O. & Chamov, N. (2004). Age, geochemistry and tectonic setting of Buqingshan ophiolites, North Qinghai–Tibet Plateau, China. *Journal of Asian Earth Sciences* **23**, 577–596.

Carswell, D. A. (1990). *Eclogite Facies Rocks*. Glasgow: Blackie; New York: Chapman & Hall, 396 pp.

Cawood, P. A., Johnson, M. R. W. & Nemchin, A. A. (2007). Early Paleozoic orogenesis along the Indian margin of Gondwana: tectonic response to Gondwana assembly. *Earth and Planetary Science Letters* **255**, 70–84.

Cawood, P. A., Wang, Y., Xu, Y. & Zhao, G. (2013). Locating South China in Rodinia and Gondwana: a fragment of greater India lithosphere? *Geology* **41**, 903–906.

Dong, Y. & Santosh, M. (2016). Tectonic architecture and multiple orogeny of the Qinling Orogenic Belt, Central China. *Gondwana Research* **29**, 1–40.

Dong, Y., He, D., Sun, S., Liu, X., Zhou, X., Zhang, F., Yang, Z., Cheng, B., Zhao, G. & Li, J. (2018). Subduction and accretionary tectonics of the East Kunlun orogen, western segment of the Central China Orogenic System. *Earth-Science Reviews*, doi:10.1016/j.earscirev.2017.12.006.

Droop, G. T. R. (1987). A general equation for estimating Fe^{3+} concentrations in ferromagnesian silicates and oxides from microprobe analyses, using stoichiometric criteria. *Mineralogical Magazine* **51**, 431–435.

Ernst, W. G. (1988). Tectonic history of subduction zones inferred from retrograde blueschist *P–T* paths. *Geology* **16**, 1081–1084.

Ernst, W. G. & Liou, J. G. (1995). Contrasting plate-tectonic styles of the Qinling–Dabie–Sulu and Franciscan metamorphic belts. *Geology* **23**, 353–356.

Gehrels, G. E., Yin, A. & Wang, X. F. (2003). Detrital-zircon geochronology of the northeastern Tibetan plateau. *Geological Society of America Bulletin* **115**, 881–896.

Han, Y., Zhao, G., Cawood, P. A., Sun, M., Eizenhofer, P. R., Hou, W., Zhang, X. & Liu, Q. (2016). Tarim and North China cratons linked to northern Gondwana through switching accretionary tectonics and collisional orogenesis. *Geology* **44**, 95–98.

Krogh Ravna, E. J. & Terry, M. P. (2004). Geothermobarometry of UHP and HP eclogites and schists—an evaluation of equilibria among garnet–clinopyroxene–kyanite–phengite–coesite/quartz. *Journal of Metamorphic Geology* **22**, 579–592.

Li, Q. L., Li, X. H., Liu, Y., Tang, G. Q., Yang, J. H. & Zhu, W. G. (2010). Precise U–Pb and Pb–Pb dating of Phanerozoic baddeleyite by SIMS with oxygen flooding technique. *Journal of Analytical Atomic Spectrometry* **25**, 1107–1113.

Li, R., Pei, X., Li, Z., Pei, L., Chen, G., Wei, B., Chen, Y., Liu, C. & Wang, M. (2018). Cambrian (~510 Ma) ophiolites of the East Kunlun orogen, China: a case study from the Acite ophiolitic tectonic mélange. *International Geology Review* **60**, 2063–2083.

Li, S., Xiao, Y., Liou, D., Chen, Y., Ge, N., Zhang, Z., Sun, S.-S., Cong, B., Zhang, R., Hart, S. R. & Wang, S. (1993). Collision of the North China and Yangtse Blocks and formation of coesite-bearing eclogites: timing and processes. *Chemical Geology* **109**, 89–111.

Li, S., Zhao, S., Liu, X., Cao, H., Yu, S., Li, X., Somerville, I., Yu, S. & Suo, Y. (2018). Closure of the Proto-Tethys Ocean and Early Paleozoic amalgamation of microcontinental blocks in East Asia. *Earth-Science Reviews*, doi: 10.1016/j.earscirev.2017.01.011.

Li, X. H., Liu, Y., Li, Q. L., Guo, C. H. & Chamberlain, K. R. (2009). Precise determination of Phanerozoic zircon Pb/Pb age by multi-collector SIMS without external standardization.

Geochemistry, Geophysics, Geosystems **10**, doi: 10.1029/2009GC002400.

Li, Z. X., Bogdanova, S. V., Collins, A. S., Davidson, A., De Waele, B., Ernst, R. E., Fitzsimons, I. C. W., Fuck, R. A., Gladkochub, D. P., Jacobs, J., Karlstrom, K. E., Lu, S., Natapov, L. M., Pease, V., Pisarevsky, S. A., Thrane, K. & Vernikovsky, V. (2008). Assembly, configuration, and break-up history of Rodinia: a synthesis. *Precambrian Research* **160**, 179–210.

Liou, J. G., Zhang, R. Y., Ernst, W. G., Rumble, D. & Maruyama, S. (1998). High-pressure minerals from deeply subducted metamorphic rocks. In: Hemley, R. J. (ed.) *Ultrahigh-Pressure Mineralogy: Physics and Chemistry of the Earth's Deep Interior. Mineralogical Society of America, Reviews in Mineralogy* **37**, 33–96.

Liu, D., Jian, P., Kröner, A. & Xu, S. (2006). Dating of prograde metamorphic events deciphered from episodic zircon growth in rocks of the Dabie–Sulu UHP complex, China. *Earth and Planetary Science Letters* **250**, 650–666.

Liu, L., Wang, C., Cao, Y. T., Chen, D. L., Kang, L., Yang, W. Q. & Zhu, X. H. (2012). Geochronology of multi-stage metamorphic events: Constraints on episodic zircon growth from the UHP eclogite in the South Altyn, NW China. *Lithos* **136**, 10–26.

Liu, L., Liao, X., Wang, Y., Wang, C., Santosh, M., Yang, M., Zhang, C. & Chen, D. (2016). Early Paleozoic tectonic evolution of the North Qinling Orogenic Belt in Central China: Insights on continental deep subduction and multiphase exhumation. *Earth-Science Reviews* **159**, 58–81.

Ludwig, K. R. (2003). *User's Manual for Isoplot 3.00: A Geochronological Toolkit for Microsoft Excel. Berkeley Geochronology Center Special Publication* **4**.

Mattern, F. & Schneider, W. (2000). Suturing of the Proto- and Paleo-Tethys oceans in the western Kunlun (Xinjiang, China). *Journal of Asian Earth Sciences* **18**, 637–650.

Meng, F., Zhang, J. & Cui, M. (2013). Discovery of Early Paleozoic eclogite from the East Kunlun, Western China and its tectonic significance. *Gondwana Research* **23**, 825–836.

Meng, F., Cui, M., Wu, X. & Ren, Y. (2015). Heishan mafic–ultramafic rocks in the Qimantag area of Eastern Kunlun, NW China: remnants of an early Paleozoic incipient island arc. *Gondwana Research* **27**, 745–759.

Meschede, M. (1986). A method of discriminating between different types of mid-ocean ridge basalts and continental tholeiites with the Nb–Zr–Y diagram. *Chemical Geology* **56**, 207–218.

Pearce, J. A. (1982). Trace element characteristics of lavas from destructive plate boundaries. In: Thorpe, R. S. (ed.) *Andesites*. New York: John Wiley, pp. 525–548.

Qi, S. S., Song, S. G., Shi, L. C., Cai, H. J. & Hu, J. C. (2014). Discovery and its geological significance of Early Paleozoic edogite in Xiarihamu–Suhaitu area, western part of the East Kunlun. *Acta Petrologica Sinica* **30**, 3345–3356.

Qi, X., Yang, J. & Fan, X. (2016). Age, geochemical characteristics and tectonic significance of Changshishan ophiolite in central East Kunlun tectonic mélange belt along the east section of East Kunlun Mountains. *Geology in China* **43**, 797–816 (in Chinese with English abstract).

Song, S., Niu, Y., Su, L., Zhang, C. & Zhang, L. (2014). Continental orogenesis from ocean subduction, continent collision/subduction, to orogen collapse, and orogen recycling: the example of the North Qaidam UHPM belt, NW China. *Earth-Science Reviews* **129**, 59–84.

Song, S. G., Zhang, L. F., Niu, Y. L., Su, L., Song, B. A. & Liu, D. Y. (2006). Evolution from oceanic subduction to continental collision: a case study from the Northern Tibetan Plateau based on geochemical and geochronological data. *Journal of Petrology* **47**, 435–455.

Song, S. G., Zhang, L. F., Niu, Y., Wei, C. J., Liou, J. G. & Shu, G. M. (2007). Eclogite and carpholite-bearing metasedimentary rocks in the North Qilian suture zone, NW China: implications for early Palaeozoic cold oceanic subduction and water transport into mantle. *Journal of Metamorphic Geology* **25**, 547–563.

Song, S. G., Niu, Y. L., Wei, C. J., Ji, J. Q. & Su, L. (2010). Metamorphism, anatexis, zircon ages and tectonic evolution of the Gongshan block in the northern Indochina continent—An eastern extension of the Lhasa Block. *Lithos* **120**, 327–346.

Song, S. G., Su, L., Li, X. H., Niu, Y. L. & Zhang, L. F. (2012). Grenville-age orogenesis in the Qaidam–Qilian block: the link between South China and Tarim. *Precambrian Research* **220–221**, 9–22.

Song, S. G., Niu, Y. L., Su, L. & Xia, X. H. (2013). Tectonics of the North Qilian orogen, NW China. *Gondwana Research* **23**, 1378–1401.

Song, S. G., Yang, L. M., Zhang, Y. Q., Niu, Y. L., Wang, C., Su, L. & Gao, Y. L. (2017). Qi-Qin Accretionary Belt in Central China Orogen: accretion by trench jam of oceanic plateau and formation of intra-oceanic arc in the Early Paleozoic Qin-Qi-Kun Ocean. *Science Bulletin* **62**, 1035–1038.

Stacey, J. S. & Kramers, J. D. (1975). Approximation of terrestrial lead isotope evolution by a two-stage model. *Earth and Planetary Science Letters* **26**, 207–221.

Stampfli, G. M., Hochard, C., Vérard, C., Wilhem, C. & von Raumer, J. (2013). The formation of Pangea. *Tectonophysics* **593**, 1–19.

Sun, S. S. & McDonough, W. F. (1989). Chemical and isotopic systematics of oceanic basalts: implications for mantle composition and processes. In: Saunders, A. D.& Norry, M. J. (eds) *Magmatism in the Ocean Basins. Geological Society, London, Special Publications* **42**, 313–345.

Topuz, G., Okay, A. I., Schwarz, W. H., Sunal, G., Altherr, R. & Kylander-Clark, A. R. C. (2018). A middle Permian ophiolite fragment in Late Triassic greenschist- to blueschist-facies rocks in NW Turkey: An earlier pulse of suprasubduction-zone ophiolite formation in the Tethyan belt. *Lithos* **300–301**, 121–135.

von Raumer, J. F. & Stampfli, G. M. (2008). The birth of the Rheic Ocean—early Palaeozoic subsidence patterns and subsequent tectonic plate scenarios. *Tectonophysics* **461**, 9–20.

von Raumer, J. F., Stampfli, G. M. & Bussy, F. (2003). Gondwana-derived microcontinents—the constituents of the Variscan and Alpine collisional orogens. *Tectonophysics* **365**, 7–22.

Wang, F., Liu, F., Schertl, H.-P., Liu, P., Jia, L., Cai, J. & Liu, L. (2018). Paleo-Tethyan tectonic evolution of Lancangjiang metamorphic complex: evidence from SHRIMP U–Pb zircon dating and $^{40}Ar/^{39}Ar$ isotope geochronology of blueschists in Xiaoheijiang–Xiayun area, Southeastern Tibetan Plateau. *Gondwana Research*, in press.

Wang, G., Sun, F. & Li, B. (2014). Zircon U–Pb geochronology and geochemistry of the mafic–ultramafic intrusion in Xiarihamu Cu–Ni deposit from East Kunlun, with implications for geodynamic setting. *Earth Science Frontier* **21**, 381–401 (in Chinese with English abstract).

Whitney, D. L. & Evans, B. W. (2010). Abbreviations for names of rock-forming minerals. *American Mineralogist* **95**, 185–187.

Wiedenbeck, M., Allé, P., Corfu, F., Griffin, W. L., Meier, M., Oberli, F., Vonquadt, A., Roddick, J. C. & Spiegel, W. (1995). Three natural zircon standards for U–Th–Pb, Lu–Hf, trace-element and REE analyses. *Geostandards and Geoanalytical Research* **19**, 1–23.

Winchester, J. A. & Floyd, P. A. (1976). Geochemical magma type discrimination: application to altered and metamorphosed basic igneous rocks. *Earth and Planetary Science Letters* **28**, 459–469.

Wood, D. A. (1980). The application of a Th–Hf–Ta diagram to problems of tectonomagmatic classification and to establishing the nature of crustal contamination of basaltic lavas of the British Tertiary Volcanic Province. *Earth and Planetary Science Letters* **50**, 11–30.

Xu, X., Song, S. G., Su, L., Li, Z. X., Niu, Y. L. & Allen, M. B. (2015). The 600–580 Ma continental rift basalts in North Qilian Shan, northwest China: links between the Qilian–Qaidam block and SE Australia, and the reconstruction of East Gondwana. *Precambrian Research* **257**, 47–64.

Xu, X., Song, S. G., Allen, M. B., Ernst, R. E., Niu, Y. L. & Su, L. (2016). An 850–820 Ma LIP dismembered during breakup of the Rodinia supercontinent and destroyed by Early Paleozoic continental subduction in the northern Tibetan Plateau, NW China. *Precambrian Research* **282**, 52–73.

Yang, J. S., Robinson, T., Jiang, C. F. & Xu, Z. Q. (1996). Ophiolites of the Kunlun Mountains, China and their tectonic implications. *Tectonophysics* **258**, 215–231.

Yang, J.-S., Wang, X.-B., Shi, R. D., Xu, Z. Q. & Wu, C. L. (2004). The Dur'ngoi ophiolite in East Kunlun, north Qinghai–Tibet Platea fragment of paleo-Tethyan oceanic crust. *Geology in China* **31**, 225–239.

Yin, A. & Harrison, T. M. (2000). Geologic evolution of the Himalayan–Tibetan orogen. *Annual Review of Earth and Planetary Sciences* **28**, 211–280.

Zhang, J. X., Meng, F. C. & Wan, Y. S. (2007). A cold Early Palaeozoic subduction zone in the North Qilian Mountains, NW China: petrological and U–Pb geochronological constraints. *Journal of Metamorphic Geology* **25**, 285–304.

Zhang, Y. Q., Song, S. G., Yang, L. M., Su, L., Niu, Y. L., Allen, M. B. & Xu, X. (2017). Basalts and picrites from a plume-type ophiolite in the South Qilian Accretionary Belt, Qilian Orogen: Accretion of a Cambrian Oceanic Plateau? *Lithos* **278**, 97–110.

Zhai, Q. G., Zhang, R. Y., Jahn, B. M., Li, C., Song, S. G. & Wang, J. (2011). Triassic eclogites from central Qiangtang, northern Tibet, China: petrology, geochronology and metamorphic *P–T* path. *Lithos* **125**, 173–189.

Zhai, Q.-G., Jahn, B.-M., Wang, J., Hu, P.-y., Chung, S.-L., Lee, H.-y., Tang, S.-h. & Tang, Y. (2016). Oldest Paleo-Tethyan ophiolitic mélange in the Tibetan Plateau. *Geological Society of America Bulletin* **128**, 355–373.

Zhu, Y., Lin, Q., Jia, C. & Wang, G. (2006). SHRIMP zircon U–Pb age and significance of Early Paleozoic volcanic rocks in East Kunlun Orogen, Qinghai Province, China. *Science in China Series D* **49**, 88–96.